Stony Brook University

Analysis and Design of Thermal Management System for

Thermoelectric Generators for Nuclear Power Plant Safety

A Thesis Presented

by

Chih Chieh Lin

to

The Graduate School

in Partial Fulfillment of the

Requirements

for the Degree of

Master of Science

in

Mechanical Engineering

Stony Brook University

May 2014

Stony Brook University

The Graduate School

Chih Chieh Lin

We, the thesis committee for the above candidate for the

Master of Science degree, hereby recommend

acceptance of this thesis.

Jon P. Longtin- Thesis Advisor
Professor Mechanical Engineering

John Kincaid- Chair
Professor Mechanical Engineering

David Hwang- Member
Assistant Professor Mechanical Engineering

This thesis is accepted by the Graduate School

Charles Taber
Dean of the Graduate School

Abstract of the Thesis

Analysis and Design of Thermal Management System for

Thermoelectric Generators for Nuclear Power Plant Safety

by

Chih Chieh Lin

Master of Science

in

Mechanical Engineering

Stony Brook University

2014

This project aims to develop thermoelectric generators (TEG)-based devices for sensing during normal and off-normal conditions in Small Modular Reactors (SMRs). Locations such as reactor core vessels, steam generators, housings of pumps, heat exchangers, and steam pipe housings in primary loop and secondary loop are potential installation sites. The heat is conducted through an adaptor to the TEGs and removed by a heat sink by means of natural convection. The electrical power generated by the TEGs is then used to drive sensors and wireless communications. Additional power can be stored in batteries or in super capacitors for emergency operations. The sensing system measures important data such as temperature, flow rate, and radiation dosage. Several experiments including the TEG test and lab-based experiment were conducted to validate the simulation and assumptions. The prototype that attaches to a 12 in. nominal size schedule 80 pipe was at 300 °C. A large natural convection heat sink is applied as the cooling solution. A thorough thermal analysis was made to assure that the heat sink temperature was below 80 °C and the TEGs temperature difference was around 100 °C. An enclosure was also presented to protect the electrical components from harsh condition.

Table of Contents

Contents

List of Figures

List of Tables

Nomenclature

A	Surface area [m^2]
D	Diameter of pipe [m]
F	View factor
g	Gravity constant [$\frac{m}{s^2}$]
h	Heat transfer coefficient [$\frac{W}{m^2K}$]
h_{opt}	Heat transfer coefficient of optimum fin spacing [$\frac{W}{m^2K}$]
k	Thermal conductivity [$\frac{W}{mK}$]
L	Fin length [m]
L_C	Corrected fin length [m]
L_i	Characteristic length [m]
L_t	Length of thermoelectric material [m] (section 2.1); Entry Length [m] (section 4.3.3)
$\dot{m}$	Mass flow rate [$\frac{kg}{s}$]
N	Number of thermoelectric element
Nu	Nusselt number
P	Perimeter [m]
Pr	Prandtl number [m]
Q	Amount of heat transfer [W]
R	Internal resistance [Ω] (section 2.1); Thermal resistance [$\frac{K}{W}$] (section 4.2 and 4.3.3)
R_L	Load resistance [Ω]
Ra	Rayleigh number

Re	Reynolds number
r_1	Inner radius of cylinder [m]
r_2	Outer radius of cylinder [m]
S	Seebeck coefficient $[\frac{V}{K}]$
S_{opt}	Optimum fin spacing [m]
T_c	Cold side temperature on thermoelectric elements [K]
T_h	Hot side temperature on thermoelectric elements [K]
T_s	Temperature of fin surface [K]
T_∞	Temperature of ambient [K]
t	Fin thickness [m]
W	Electrical power output [W]
x	Wall thickness [m]
y	Heat sink length [m]
Z	Figure of merit$[\frac{1}{K}]$

Greek symbols

α_n	N-leg Seebeck coefficient $[\frac{V}{K}]$
α_p	P-leg Seebeck coefficient $[\frac{V}{K}]$
β	Coefficient of volume expansion $\left[\frac{1}{K}\right]$
ΔT	Temperature difference $[K]$
ε	Emissivity
η	Fin efficiency
σ	Stefan-Boltzmann constant
ν	Kinematic viscosity $[\frac{m^2}{s}]$

Acknowledgments

I would like to express my gratitude to Professor Jon P. Longtin for encouraging my research and for his valuable guidance and academic support during the work on this thesis. I have learned a lot under his supervision. His advice has been a great help in this project.

I would also like to thank Professor David Hwang and Professor Lei Zuo for giving insightful suggestions and comments. Their strictness with research make me a good example for me to follow in the future of my career.

Many thanks are also due to my labmate, Hanfei Chan, who contribute his expertise in electrical engineering. Tao He and Mahder Tewolde have been supportive in thermal design and experiment. Without their help, this project would not have been possible.

1 Introduction

1.1 Motivation

Nuclear energy was expanding fast because of the increasing oil price, environmental effects, cost of electricity, and growing energy demands. The United States provides 19% of electricity by nuclear energy. However, nuclear plants accidents (Chernobyl, Three Mile Island, and Fukushima Daiichi) have cast a negative shadow on the history and future of nuclear power [1]. These events had heightened public concerns of safety issues, therefore, the demand for new nuclear plants dropped quickly in the mid-1970s [2]. A total lack of power at the plant is one of major concerns of nuclear plants' development. As seen in the Fukushima accident, the on-site and offsite power was lost because of a tsunami. As a result, the sensing systems for updating important status inside the plant became unavailable.

The offsite power source, which is often supplied from electric grids that are far away from the nuclear power plant, is the primary power source during normal operation. The onsite power sources are diesel generators and back-up batteries that will be used when an offsite power source is not available. If all these power sources become unavailable, a station blackout results. A station blackout disables most of the systems relied on for core cooling. In fact, loss of all AC power contributes to more than 70 percent of the overall risk at some plants [3]. And loss of offsite power in nuclear plants is one of the most frequent incidents in the U.S. A total of 42 separate power-out conditions in the U.S from 1997 to 2004 have been recorded. Among these incidents, 24 had caused critical operation conditions and 18 more resulted in shutdown conditions. These incidents had the potential to become irreversible accidents if the onsite power source had also failed.

In the Fukushima Daiichi accident, the earthquake cut off the offsite power source, and the onsite emergency diesel generators were also disabled because of the tsunami. After the backup batteries ran out, the nuclear plant was in a station blackout. This might lead to a malfunction of the cooling system. In light water reactors, for example, peak core temperatures can reach 1,100 K in less than 30 minutes if the cooling system becomes unavailable. At this temperature, cladding of the fuel

rods can burst [4]. As a result, it is vitally important to maintain important parameters available during off-normal conditions.

It might be too idealistic to ensure that no nuclear incident happens, but people can still be dedicated to minimize the damage by improving the ability to manage an emergency. A reliable and self-powered monitoring device that measure parameters (even operates actuations during off-normal situations) can provide important parameters to help operators understand the system status in the plants during normal and off-normal situations. And the most importantly, this device should be sustainable in harsh environments, such as in water, fire, shock, and high-dose radiation exposure. Therefore, an aircraft black box-like protection shell is also included in this device.

1.2 Project Summary

A self-powered and harsh condition-sustainable monitoring device, which provides parameters to operators during normal and off-normal situations in nuclear power plants is our objective. The following are the works and surveys included in this project.

1. Explicit survey for Small Module Reactor: The important parameters such as temperature, diameter, and accessibility are collected at several potential locations.
2. Introduction to operating principal of TEGs: Available commercial products and their specification are also presented.
3. Radiation effect: Radiation level in nuclear power plants and its effects on electronic devices and TEGs are discussed.
4. Enclosure for harsh conditions: Environmental conditions in harsh conditions and possible enclosure materials for protecting the device are discussed.
5. Thermal analysis in both analytical and Computer Aided Engineering method: This part mainly discusses about the adaptor and heat sink design and the thermal expansion of the steam pipe.
6. Lab-based experiments and field testing result: In order to validate our analysis result, two lab-based experiments before the installation of the device in the power plant.

1.3 Thesis Organization

The motivation and summary of this project are included in the chapter 1. Backgrounds of the project such as thermoelectric generators, small modular reactors, environmental conditions, and sensing requirements are introduced in chapter 2. Then, reactors types and formats, temperature estimates, down-selection of target installation sites, and environment protection are discussed in chapter 3. Both analytical and CAE analyses and designs of the adaptor and the heat sink are made in chapter 4. In Chapter 5, the setup and design of three experiments including TEG test, laboratory-based test, and field-based test are introduced. Results from chapter 4 and 5 are shown and discussed in chapter 6. Finally, the conclusion along with the future work of this project is presented in chapter 7.

2 Background

2.1 Thermoelectric Generators

Thermoelectric generators are devices that covert heat into electrical power by using the Seebeck effects, which occurs among thermoelectric materials. They can be applied in locations with a large amount of heat, and are especially suitable for applications where conventional heat engines are not feasible, e.g. spacecraft. Heat energy harvesting for gas pipe, cars and other automobiles are also very common in the use of TEGs. The Seebeck effect on TEGs occurs when there is a temperature difference across a thermoelectric material, which causes a voltage drop because charge carriers (electrons (e^-)in n-type materials and holes (h^+) in p-type materials) at the hot side moves to the cold side [5].

As shown in Figure 2-1, a TEG consists of p-type and n-type thermoelectric elements placed between conductive layers. The entire assembly is then sandwiched between two ceramic substrate. Heat transfer though thermoelectric components producing an electrostatic potential thus causes current flow.

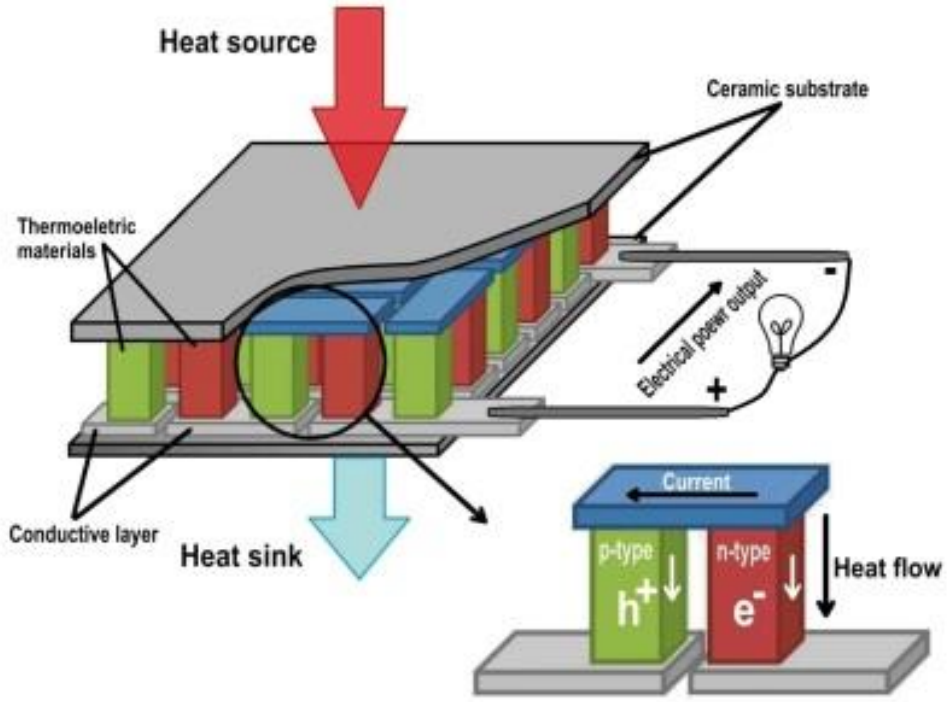

Figure 2-1: A thermoelectric generator [6].

The efficiency of a TEG depends on the efficiency of its thermoelectric material, which is determined by the figure of merit, Z (1/K)

$$\boldsymbol{Z = \frac{\sigma S^2}{k}} \tag{1}$$

where S is the Seebeck coefficient (V/K), σ is the electrical conductivity (Ω·m), and k is the thermal conductivity (W/m·K). A lower thermal conductivity means a larger temperature gradient, which results in a larger power output. A Higher electrical conductivity means less resistance when the charge carriers flow across the thermoelectric materials, which also increases the power output. The output voltage of the TEG is proportional to the number of thermoelements (N), the temperature difference between the cold-side temperature (T_c), and the hot-side temperature (T_h).

$$\boldsymbol{V = \frac{SN(T_h - T_c)}{1 + 2\frac{k_t}{k_c}\frac{L_c}{L_t}}} \tag{2}$$

where L_t and k_t are the length and the thermal conductivity of the thermoelectric material. L_c and k_c are the thickness and thermal conductivity of the ceramic substrate. The current of the TEG can be calculated from

$$\boldsymbol{I = \frac{(\alpha_p - \alpha_n)\Delta T}{R_L + R}} \tag{3}$$

where α_n and α_p are the n-leg Seebeck coefficient and p-leg Seebeck coefficient. R_L and R are the load resistance and internal resistance of the TEG [7, 8]. Finally, the power generated from TEG is

$$\boldsymbol{W = I^2 R_L} \tag{4}$$

Generally, a commercial TEG can generate around 5 watts with an efficiency of 4.5 % if adequate heat source and environment condition applied. The ideal temperature difference for optimal performance for a commercial TEG is around 200 °C. The maximum working temperature is normally below 300 °C. Figure 2-2 shows that other thermoelectric materials such as La_3Te_4 and $Yb_{14}MnSb_{11}$ can tolerate high temperature but are not commercialized yet [9].

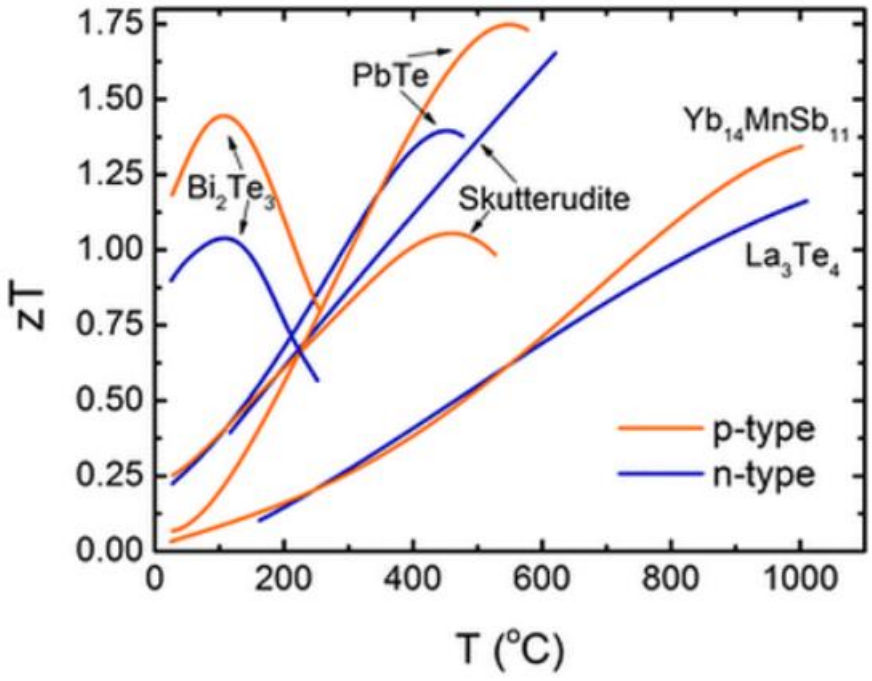

Figure 2-2 Working temperatures and figures of merit of thermoelectric materials [9]

2.2 Small Modular Reactors

The target power plants is the Small Modular Reactors (SMRs). They are a new generation of nuclear reactor that are more flexible, standardized, and safer. The SMRs, which are built in modular at factories, are able to be shipped by truck, train, or barge.

There are more than 12 advanced SMRs currently being developed and could be implemented before 2020 [1]. Major differences between SMRs and conventional nuclear reactors are that SMRs have higher degree of innovation features and also are able to meet specific requirement of power and space available of target market. As a result, SMRs are especially suitable for remote and isolated areas where large generation capacity nuclear reactors are not needed and replacement for the old and decommissioned fossil fuel plants. Factors that make SMRs competitive are listed as follows [10],

Modularity: Major components of SMRs are able to be fabricated in factories and shipped to target locations while conventional nuclear reactors required field works. This reduces the onsite preparation and construction time, and hence lower capital investment costs.

Siting Flexibility: SMRs can provide power for areas where large plants are not needed. SMRs are especially suitable for remote and isolated areas where large generation capacity are not needed and replacement for the old and decommissioned fossil fuel plants.

Nonproliferation: One of the major concerns for selling nuclear power plant to foreign countries is that there is a potential of the development of nuclear weapons. SMRs provide safety and nonproliferation nuclear energy resource to other countries. This approach could help to minimize the transportation and handling of nuclear material. These SMRs are sealed and transported to sites, and then returned to the factory for defueling.

International Market: The United State can also profit from the great interests from selling SMRs to countries which don't have the technology to build their own nuclear power plants.

Advanced features for safety concerns: Many advanced technologies have been applied on SMRs including (1) inherent safety features (e.g. generators located relative higher than core to

enhance natural circulation flow), (2) multiple-reactor shutdown system (e.g. control rod insertion driven by electric motor, gravity, and springs), (3) reactor vessel passive cooling system (e.g. redundant and diverse active and passive core cooling systems).

Safety is the major concern for SMRs. SMR manufacturers are still seeking for more safety features. The TEG-based sensor is a very promising feature that reinforces the safety of SMRs. All designs in this thesis are made to accommodate SMRs.

2.3 Environmental Conditions

The environment under a normal condition in SMRs has a slightly higher ambient temperature and radiation dosage compared to common indoor environments. The ambient temperature near steam pipe is around 35 °C in summer and 20 °C in winter. During an off-normal condition, on the other hand, there are mainly four scenarios might happen:

(1) Water: The installation location might be invaded by water because of leakage of pipes and fire sprinkler system, or even flooding caused by tsunami. Moreover, many advanced SMRs are built underground in order to utilize gravity for passive cooling system, which means a complete immersion might also happen. Therefore, a waterproof enclosure design is needed in this project.

(2) High temperature: Explosion of generators or core damage will increase the ambient temperature which could disable or even melt the device. In a core meltdown scenario, reactor temperature could be increased from 600 K to 1100 K within 2.5 hours [4].

(3) Shock: Shock caused by explosion or earthquake could physically damage the device. As a result, a firm protection layer made by hard metal is included in the enclosure.

(4) Radiation exposure: The leakage of alpha, beta, gamma and neutron radiation caused by reactor shell damage could damage the circuit board [11]. Therefore, an extra shield for blocking radiation is required in this project. Different electronic components can handle varying degrees of radiation exposure, as shown in Table 2-1.

Table 2-1 Threshold of radiation for different electronic components [12]

Component type	Damage threshold (Gy)
Resistors	10^2 — 10^6
Capacitors	10^2 — 10^8
Inductors	10 — 10^6
IC	10^2 — 10^4
Voltage regulator	10^3 — 10^6

Also, different locations and operating conditions result in different radiation levels (Table 2-2)

Table 2-2 Radiation level at different locations in nuclear plants [13]

Location	State of reactor	Gamma dose rate (Gy/h)	Neutron dose rate (Gy/h)
Inside the core	On load	10^7	10^7
	Shut-down	10^4	10^{-1}
Outside the radial shield	On load	10^2	10
	Shut-down	10^{-3}	Negligible
Above the pressure dome	On load	10	1
	Shut-down	$5 \cdot 10^{-3}$	Negligible
Coolant loop	On load	$5 \cdot 10^{-1}$	Negligible

Although radiation generally causes negative effects on electronic circuits, it is not undesirable for TEGs. The Seebeck coefficient is actually improved after radiation exposure [14].

2.4 Sensing Requirements

The primary coolant loop is one crucial location that must be examined by reliable sensors, in other words, it is an ideal location to install this TEG powered sensing system. Important parameters such as (1) temperature of the coolant entering the reactor, (2) temperature of the coolant leaving the reactor, (3) temperature of the coolant at other positions in the reactor, (4) flow rate of coolant into and out of the reactor, (5) flow rate of coolant in various coolant channels in the reactor, (6) the radioactivity of the coolant after leaving reactor. As a result, temperature sensors, flowmeters, and nuclear radiation sensors are three basic requirements [15]:

1. Thermocouples are the most reliable and broadly used temperature sensors. They are devices that generates a voltage which is proportional to the temperature difference between hot and cold junctions.
2. Flowmeters are considered to consist of a primary element, which contacts the flowing fluid, and a secondary element, which indicates information. In a differential-pressure type flowmeter, the primary element is an obstruction placed in the pipe to create a pressure drop such as Venturi Tube. The secondary element is a device to measure this pressure drop and convert it to rate of flow.
3. Ionization chambers are the most common radiation sensors in nuclear power reactors. Ionization chambers measure the electric charge of ions and electrons that result from the interaction of incident radiation and secondary radiation. The quantity of collected charge is a measure of radiation.

3 Requirements Survey

3.1 Reactors Types and Formats

Nuclear fission reactors can be classified into four types by their coolant and moderator materials. These types of nuclear reactors have been used in producing commercial electricity around the world [16].

(1) **Gas cooled and graphite moderated:** Early stage of nuclear reactor type that are graphite moderated and gas cooled. Magnox reactors, which were all decommissioned, are named after the magnesium alloy used to encase the uranium fuel. This type of reactors is cooled by carbon dioxide gas which then provide the heat for converting water to steam in s steam generator. Typical reactor temperature and pressure for this type are 360 °C and 300 Psia.

(2) **Heavy water cooled and moderated:** CANDU is the only commercial reactor that uses heavy water as moderator. Heavy water is pressurized to prevent boiling and then pumps to a steam generator to converting light water to steam. This type of reactors allows the use of natural uranium. But the high cost of heavy water is a tradeoff against the reduced fuel costs.

(3) **Light water cooled and moderated:** The most common type of reactors that uses highly enriched U235 as fuel. Pressurized water reactors (Figure 3-1) and boiling water reactors are the two general types of light water cooled and moderated reactors. In pressurized water reactors, the primary coolant is pumped under high pressure to the reactor in order to prevent water from boiling, while BWRs allow water within reactor to boil and directly generate steam for power generator.

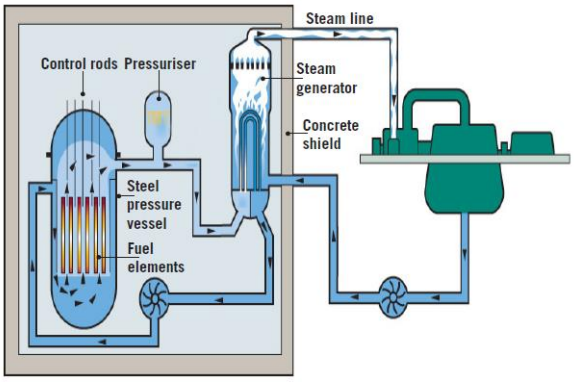

Figure 3-1 Pressurized water reactors [16]

(4) **Light water cooled and graphite moderated:** Similar to light water cooled and moderated reactors except using graphite as moderator. Many of this type have been constructed in USSR. There are 11 this type of reactors operating in Russia in the year of 2013.

3.2 Temperature Estimates

Among these types of reactors, the light water cooled and moderated reactor is the most common type for SMRs because it is relatively cheap, simple, and safe. Other new designed reactors using different materials as coolants, e.g. liquid metal, gas and molten salt, are also being developed for higher temperature operation. As presented in Table 3-1, temperatures of SMRs range from 150 °C to 750 °C.

Table 3-1 Temperature estimates at different SMRs [17]

	KLT-40S	NuScale	4S	mPower	SMART
Thermal/Electric Output (MW)	150/35	160/48	30/10	400/125	330/100
Core inlet/outlet nozzle temperature (°C)	280/316	248/289	310/355	297/321	295.7/323
Steam generator inlet/outlet temperature (°C)	170/290	Not specified	210/453	163/300	200/298

Specifically, Figure 3-2 shows local temperatures at different locations in the 4S. As one can see, the temperature of coolant in the primary loop is 355 °C before it flows into reactor core. After absorbing the energy from nuclear fission, the temperature of coolant can be as high as 510 °C. The coolant in the secondary loop is heated up from 310 °C to 485 °C by gaining energy from heat exchanger. And the coolant (485 °C) carries the heat to the steam generator which heats up the coolant in the steam water loop from 210°C to 453°C.

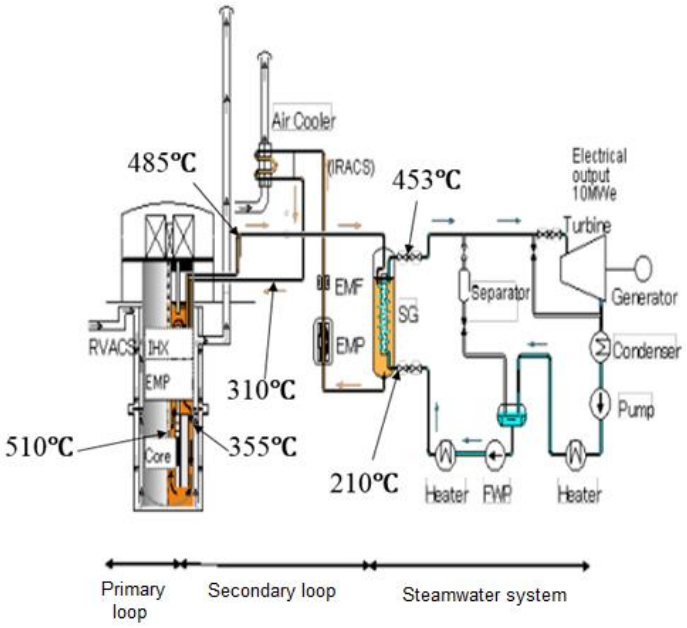

Figure 3-2 Local temperature at different locations in 4S [16]

3.3 Down-Selection of Target Installation Sites

At the very stage of the project, several potential candidates are chosen such as reactor core vessels, steam generators, housings of pumps, heat exchangers, and steam pipe housings in primary loop and secondary loop. To narrow down target installation locations, four primary criteria are used to determine the ideal location.

(1) Accessibility and safety concerns: Reactor core vessels and heat exchangers inside reactors are almost impossible to access. Also, the radiation level is so high that could damage the device.

(2) Temperature: Temperatures of target locations must be close to TEGs working temperature. As mentioned in section 3.2, the maximum temperature inside SMRs is up to 750 °C. A commercial TEG module, however, usually has a maximum working temperature of 300 °C. Extra works such as designing a high thermal resistance coupler or using non-commercialized TEGs will be needed to accommodate this temperature mismatch.

(3) Space: Target locations should have enough space for installing the heat sink and the electronics package. Locations such as reactor core vessels and the heat exchanger inside reactors would have very limited space.
(4) Shape and surface roughness: A round shape is desirable for mounting and a flat and smooth plane has a less thermal contact resistance. Housings of pumps usually have fins on them which make this location undesirable.

As a result, reactor core vessels, the heat exchanger inside reactors, and housings of pumps are out of question. Steam pipes in primary loop and secondary loop become ideal locations because

- Round surface which is easy to mount
- Made by steel which can be polished
- Low dose of radiation
- Able to access during annual maintenance

3.4 Environment Protection

The environment protection design is crucial in this project. The device is expected to survive in any possible scenarios including water, high temperature, shock, and radiation exposure, which are considered to be harmful for the circuit board and TEGs. Therefore, a multilayer enclosure for protecting the circuit board and TEGs from damaging by scenarios mentioned above is introduced. The idea is basically derived from aviation "black box" [18]. Layers of the enclosure for each scenario are stated below.

(1) Waterproof layer: Even a small drop of water can damage of TEGs and other electronic devices. Hence a waterproof layer which provide complete sealed environment is very important. A complete sealed stainless steel/titanium layer can act as a perfect water insulated wall.
(2) Thermal insulation layer: As mentioned in section 2.3, temperature in reactors can reaches 1100 K. As a result, a thick layer made by dry silica which provides high-temperature insulation is needed. This makes the device inside the enclosure possible to tolerate fire at 1,100 °C for one hour.

(3) Shock resistant layer: Shock or collision caused by earthquake or explosion can be resisted by the stainless steel/titanium layer.

(4) Radiation shielding layer: Multiple inner layers will be used for preventing the device from damaging by radiation. High-temperature polymers including Polysulfone (PSU) / Polyethersulfone (PES) / Polyphenylsulfone (PPSU) capable of blocking alpha and beta radiation. And a lead sheet can be used to block gamma radiation.

The multilayer protection enclosure is shown as Figure 3-3,

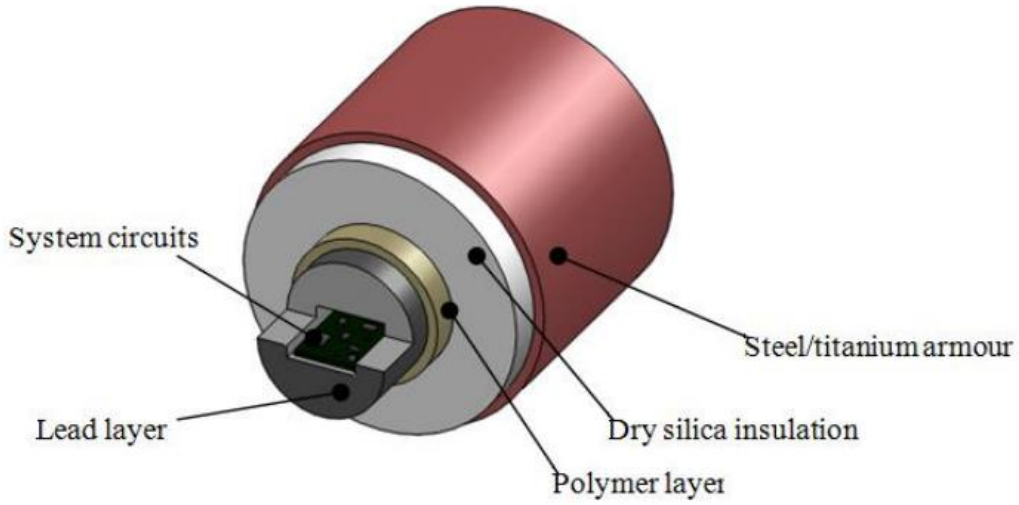

Figure 3-3 Protection enclosure design [12]

4 Thermal Analysis and Design

4.1 TEG Requirements and Performance

The required performance of TEGs is based on the power requirement of entire electrical components. The device is designed to be able to switch between normal-operation mode and sleep mode for saving power. The extra power generated from sleep mode is stored in rechargeable batteries or super capacitors for actuation such as opening a valve.

There are mainly five key components in the device, i.e. DC/DC converter, microcontroller, wireless transceiver, conditioning chip, and other electronics. The estimated power requirements for these five components are shown in Table 4-1.

Table 4-1 Estimated power requirement of each electronic component

	Estimated Power Requirement	
Component	Sleep Mode (W)	Normal-Operation Mode (W)
DC/DC Converter	<0.01	0.01-0.10
Microcontroller	<0.01	0.05-0.15
Wireless Transceiver	<0.10	0.10-0.50
Conditioning Chip	<0.01	0.01-0.10
Other Electronics	<0.01	0.01-0.15
Total	**<0.14**	**0.18-1.00**

As one can see, the total power requirement under normal operation mode is less than 1 W, which wireless transceiver consumes 50% of the total power. Sleep mode, on the other hand, only requires less than 0.14 W. Based on this estimated power requirement, the equivalent capacity of the power storage system should be more than 720Wh to ensure that the whole system can survive longer than one month when no heat is available.

4.1.1 Matching with Available Products

Based on the surveys of temperature estimates at target locations and TEG performance and requirement, a final decision of TEG product was made. Four available commercial TEGs, which are close to our demand, are listed in Table 4-2 along with their sizes, working temperatures, and performances.

Table 4-2 Specifications of commercial TEGs [19] [20] [21] [22]

Company	Hi-Z Technology		TECTEG		Marlow Industries	Custom Thermoelectric
Production	Hi-Z 14	Hi-Z 2	12610-5.1	1263-4.3	TG12-8-01L	1261G-7L31-05CQ

Size (cm)	6.27×6.27	2.9×2.9	4.0×4.0	3.0×3.0	4.0×4.5	4.0×4.0
Cold Side Temp (℃)	30	30	30	30	50	30
Hot Side Temp (℃)	230	230	300	300	230	300
Open Circuit Voltage (V)	3.5	6.5	7.8	10.7	9.4	N/A
Match Load Voltage (V)	1.7	3.3	3.9	5.3	5.3	3.63
Power (Watts)	14	2.5	5.1	5.2	8.0	7.15

In general, all these four TEG products match the demand. However, Hi-Z 14 and 1261G-7L31-05CQ have relative low voltages. Hi-Z 2 from Hi-Z Technology and 1263-4.3 from TECTEG have been selected in this project.

4.2 Thermal Analysis – Analytical

In previous chapters, we identified temperature of steam and ambient, therefore, thermal analysis and design can be deployed. Before simulating the design by CAE software, we had a basic analysis based on the thermal resistance network. The general format of thermal resistance is defined as Equation 5. Equation 6, Equation 7, and Equation 8 are thermal resistance for conduction, convection, and conduction in cylinder wall, respectively [23].

$$\boldsymbol{R} = \frac{\boldsymbol{\Delta T}}{\boldsymbol{Q}} \tag{5}$$

$$R_{conduction} = \frac{x}{kA} \tag{6}$$

$$R_{convection} = \frac{1}{hA} \tag{7}$$

$$R_{cylinder} = \frac{ln(\frac{r_2}{r_1})}{2\pi kL} \tag{8}$$

The thermal resistance network is particular useful at the first step of thermal design. It helps designers roughly estimate the temperature at each location, and thus, perceiving the basic idea of the size of each component. Figure 4-1 is the thermal resistance of the entire system. The adaptor is constructed from three parts including the coupler, the connecting rod, and the heat conducting plate (Figure 4-2). The connecting rod is assembled by the sleeve and the rod (Figure 4-3). Four thin slots on the sleeve are for adjusting the total length of connecting rod.

Figure 4-1 Thermal resistance of the entire system

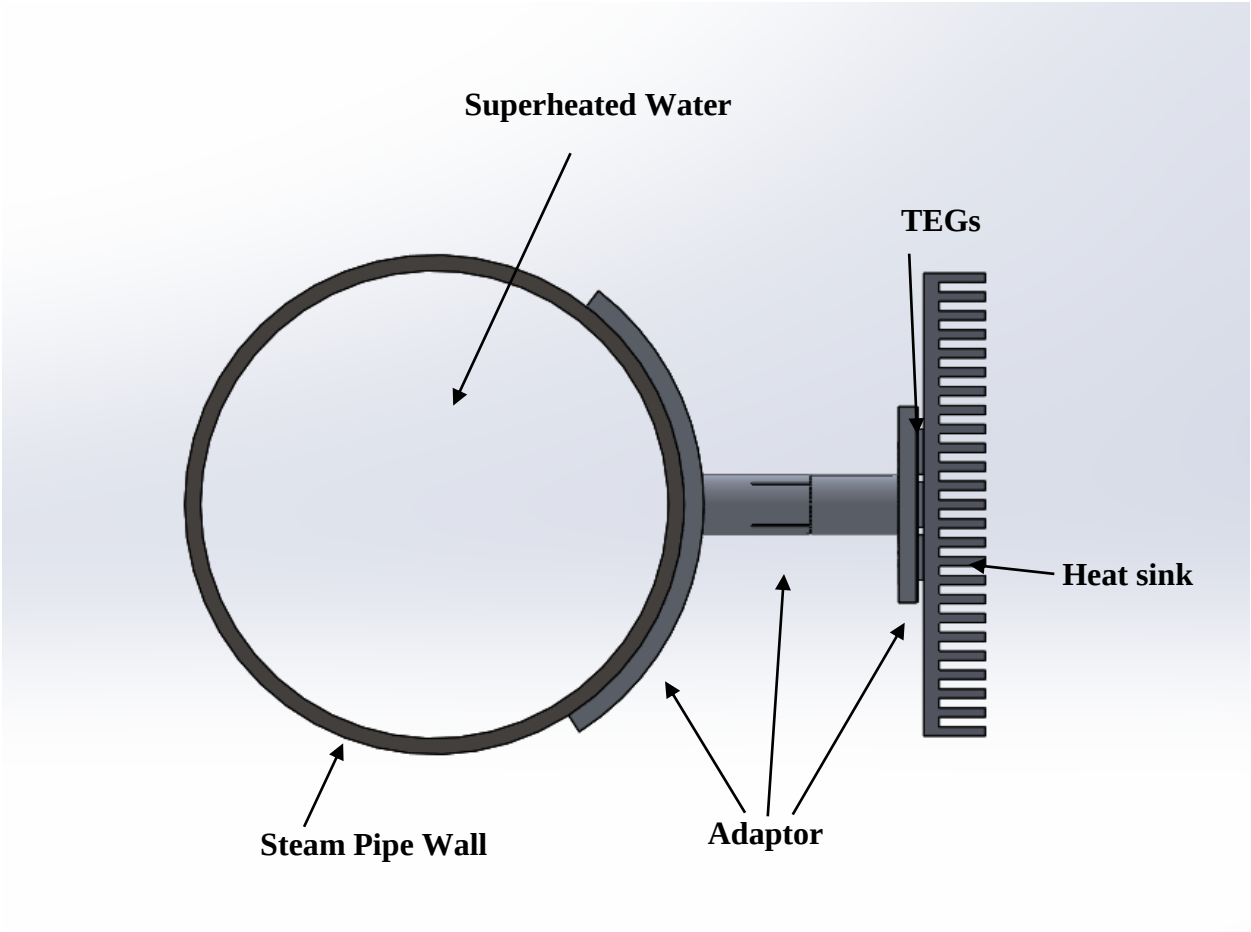

Figure 4-2 Entire thermal design

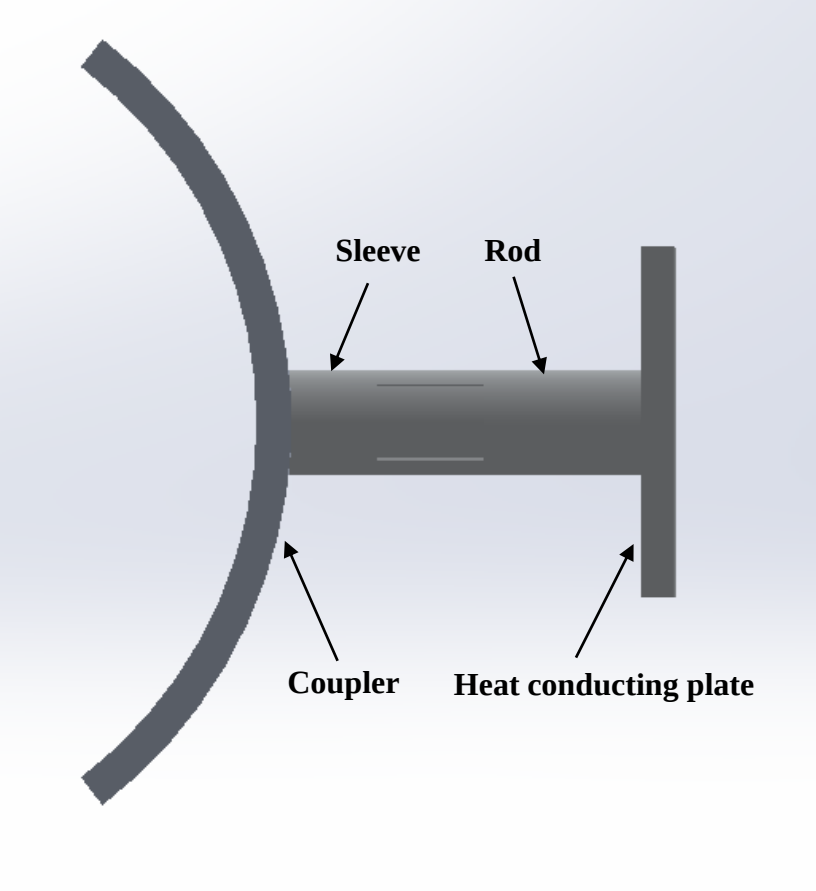

Figure 4-3 Adaptor design

The 4000kPa and 320°C superheated water flows inside the 12 in. nominal size schedule 80 pipe made by AISI 1018 (mild steel). The aluminum 6061 is also decided to be used as the material of adaptor before analysis because of its good machinability and low unit price. Four HZ-2 from Hi-Z Technology are sandwiched between the heat conducting plate and the heat sink. Ambient temperature is assumed to be 30°C.

Procedures of this analysis including (1) identify the goal temperature difference of TEGs, (2) total thermal resistance of the entire network, (3) determine an ideal heat sink, and (4) design the adaptor.

All information required to calculate thermal resistance are listed as follows,

- **TEG (HZ-2)**

Thermal conductivity: 2.4 W/m·K

Thickness: 0.51 cm

Thermal contact area: 8.65 cm^2

Required temperature difference: 100 °C

- **Adaptor (Aluminum 6061)**

Thermal conductivity: 173 W/m·K

Thickness: To be determined

Thermal contact Area: To be determined

- **12 in. nominal size schedule 80 pipe (AISI 1018)**

Thermal conductivity: 52 W/m·K

Outer diameter: 12.75”

Inner diameter: 11.38”

Thermal contact Area: To be determined

- **Superheated water**

Temperature: 320 °C

Pressure: 4000kPa

Kinematic viscosity: 2.67 $\times 10^{-7}$ kg/m·s

Mass flow rate: 7.65 kg/s

Prandtl number: 0.986

Thermal conductivity: 0.0422 W/m·K

The superheated water inside the steam pipe has a Reynolds number of 1.46×10^6 which is greater than 10^5 which indicates it is a turbulent flow. The entry length is can be defined as

$$\boldsymbol{L_t = 10D} \tag{9}$$

, which is much shorter than the total length of this pipe. Hence, we can assume fully developed turbulent flow. The Nusselt number can be determined by Equation 10 [24] [25] [26].

$$\boldsymbol{Nu = 0.023 Re^{0.8} Pr^{\frac{1}{3}}} \tag{10}$$

$$Re = \frac{4\dot{m}}{\nu \pi D} \tag{11}$$

, where $\dot{m}$ is mass flow rate, ν is kinematic viscosity, and D is the diameter of the tube.

Then the heat transfer coefficient can be obtained by

$$\boldsymbol{h = \frac{k}{D} Nu} \tag{12}$$

4.3 Thermal Analysis – CAE

4.3.1 Geometry Simulation with SolidWorks

The Computer Aided Design (CAD) helps engineers verify the feasibility of the design and provide an easier way to collaborate with machinists. The Computational Fluid Dynamics (CFD) software and other computer simulation software are also compatible with CAD drawing software such as SolidWorks and AutoCAD. Dimensions of mechanical drawings in this project are based on the result acquired from the analytical analysis. Figure 4-4 presents the three dimensional drawing including steam pipe, adaptor, TEGs, and heat sink. Each part has to be built separately in Solid-Works for being considered as an individual part with different materials while performing a simulation in a CFD software.

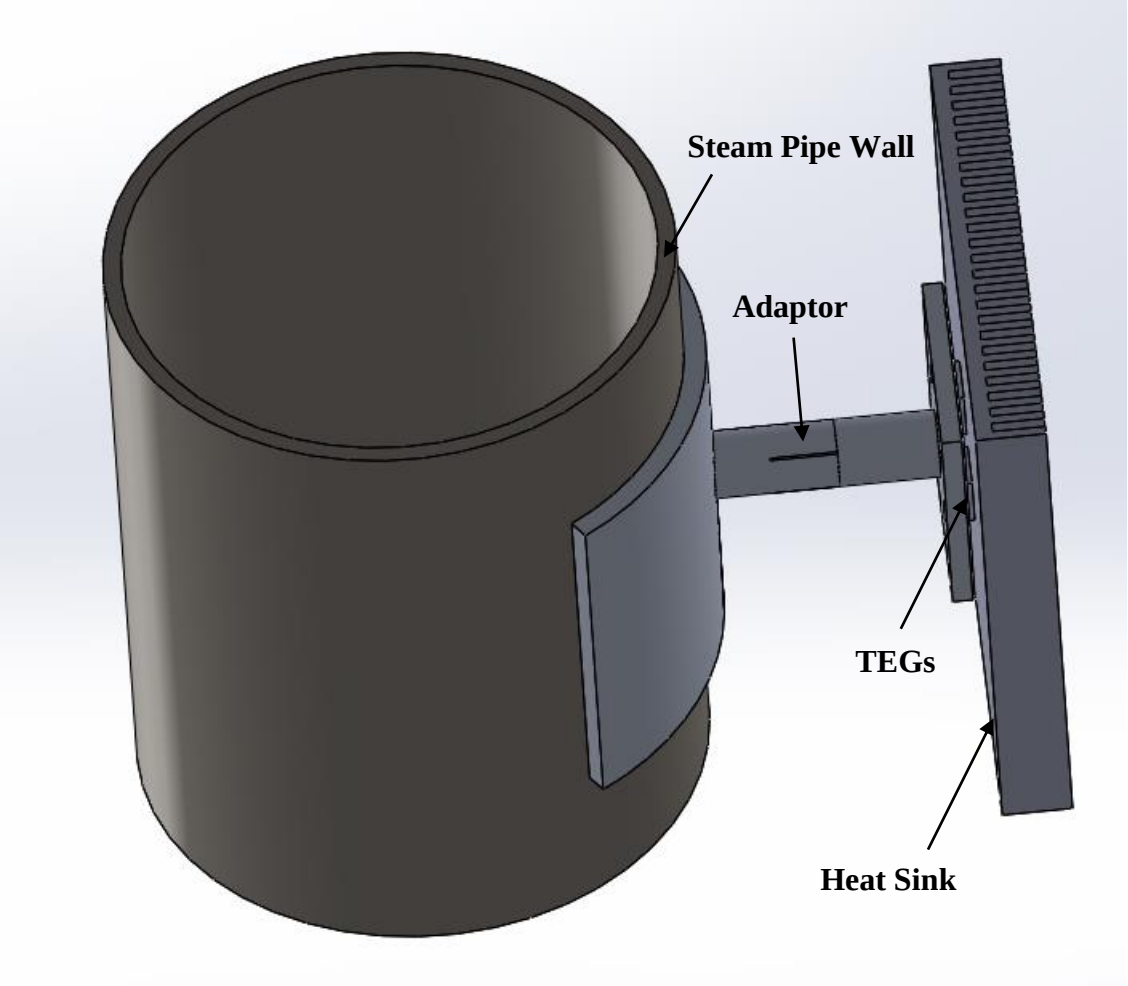

Figure 4-4 Three dimensional drawing

4.3.2 Analysis with COMSOL

After having the basic idea of heat conduction problem by thermal resistance network, we implemented a computational analysis by using a Computer-Aided Engineering (CAE) software, COMSOL. This can provide an accurate result for verifying the analytical results and understanding detailed information about temperature distribution along the entire design. The procedures of this simulation are listed as follows,

- Import the geometry drew from SolidWorks.

- Define the materials.
- Identify and define boundary conditions.
- Create mesh
- Compute and analysis result

Material properties are usually provided by CAE software but properties for some specific materials, i.e. thermal electric materials, have to be defined manually. In this work, one Hi-Z 2 is considered as a single solid block with thermal conductivity of 2.4 W/m·K, which is claimed by Hi-Z technology.

The Computer-Aided Engineering is usually performed by computer clusters since massive computational power is required. However, a very close result can also be obtained by simplifying the problem. For the heat convection problem of superheated water in this project, the heat transfer coefficient is obtained by the analytical method. TEGs are also assumed to be single solid block instead of simulating each thermal electric material as shown in section 2.1. As for heat sink by means of external natural convection, it can be solved by empirical correlation equations instead of solving the real convection problem, which is coupled with fluid dynamics.

4.3.3 Heat Sink Design

The heat sink design is the catch in this analysis. A force convective heat sink is out of question because an extra fan consumes more electricity and makes our device less reliable. Natural convection heat sink becomes the only option. At the very beginning of this project, a customized heat sink for fully satisfying our demand (size-wised and performance-wised) is designed. We had performed several analyses based on both empirical correlation equations and the CAE method. A typical vertical heat sink configuration is shown in Figure 4-5. *t* and *S* refer to the fin thickness and spacing, respectively, while *L* and *H* refer to the heat sink length and fin height, respectively.

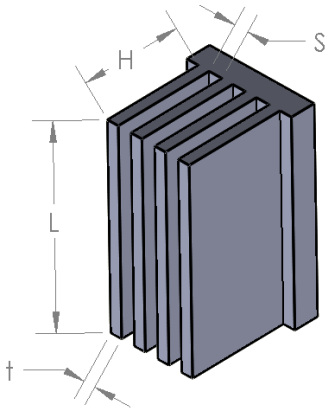

Figure 4-5 Vertical heat sink configuration

The optimum fin spacing for a fixed length (L) vertical natural convection heat sink determined by Bar-Cohen and Rohsenow [27] is

$$\boldsymbol{S_{opt} = 2.714 \frac{L}{Ra_y^{0.25}}} \tag{13}$$

$$Ra_y = \frac{g\beta(T_s - T_\infty)y^3 Pr}{\nu^2} \tag{14}$$

, where β is coefficient of volume expansion and y is heat sink length (L). The heat transfer coefficient (h) in this case is

$$\boldsymbol{h_{opt} = 1.307 \frac{k}{S_{opt}}} \tag{15}$$

, where k is heat transfer conductivity of air. The heat dissipation by heat sink (Q) is

$$\boldsymbol{Q = h_{opt} A (T_s - T_\infty)} \tag{16}$$

, where A is the surface area of heat sink, T_s is the heat sink surface temperature, and T_∞ is the ambient temperature. In this correlation, fins are assumed to be isothermal. Therefore, we need to apply fin efficiency equation for more precise result. The fin efficiency (η) for straight rectangular fins is defined as [28]

$$\boldsymbol{\eta = \frac{tanh(mL_c)}{mL_c}} \tag{17}$$

, where

$$\boldsymbol{m = \sqrt{\frac{2h}{kt}}} \tag{18}$$

$$L_c = L + \frac{t}{2} \tag{19}$$

The thermal resistance for heat sink under the non-isothermal condition thus becomes

$$\boldsymbol{R = \frac{\eta Q}{T_s - T_\infty}} \tag{20}$$

By the analysis above, we can determine the ideal heat sink design for the optimum performance. The performance of this heat sink is also verified by CAE analysis.

However, we chose to buy a commercial product which is close to our requirement eventually because it is time consuming and expensive to machining a customized heat sink. To validate the performance that heat sink manufacturer claims, we also performed both analytical and CAE analyses.

For analyzing the commercial heat sink analytically, we applied the correlation for natural convection on vertical wall (Equation 21) [29], hot surface facing upward (Equation 22) [30], and hot surface facing downward (Equation 23) [31].

$$\boldsymbol{Nu = \{0.825 + \frac{0.387Ra^{1/6}}{[1 + (0.492/Pr)^{9/16}]^{8/27}}\}^2} \tag{21}$$

$$Nu_L = 0.54{Ra_L}^{0.25} \tag{22}$$

$$Nu_L = 0.27{Ra_L}^{0.25} \tag{23}$$

$$Ra_L = \frac{g\beta(T_s - T_\infty){L_i}^3 Pr}{\nu^2} \tag{24}$$

$$L_i = A/P \quad (25)$$

, where A is area and P is perimeter.

We also applied the fin efficiency equation (Equation 17) mentioned above since this correlation is also in isothermal condition.

A CAE simulation was also made to compare with the analytical result for customized heat sink. The boundary condition and material properties are listed below,

Fin base temperature: 80 °C

Ambient temperature: 30 °C

Ambient pressure: 1 atm

Thermal conductivity of heat sink: 173 W/m·K

Thermal conductivity of air at 30 °C: 0.02588 W/m·K

Kinematic viscosity of air at 30 °C: 1.608×10^{-5} m^2/s

Prandtl number of air at 30 °C: 0.7282

Emissivity of heat sink surface: 0.77

5 Experimental Validation

5.1 TEG Testing

Experiments for TEG testing had been made for confirming the performance claimed by manufacturer. As shown in Figure 5-1, the test stand consisted of four cartridge heaters implanted in the copper block. Four cartridge heaters which provide 800 W of heat were connected to a temperature controller (Figure 5-1) with a thermocouple for feedback.

Figure 5-1 Temperature controller

On the top of the test stand, water cooling blocks were mounted for removing heat which has a thermal resistance of 0.011 ˚C/W. TEGs were sandwiched between water blocks and copper block. Hi-Z 2 from Hi-Z Technology and 1263-4.3 from TECTEG were selected in this test.

As shown in Figure 5-2, a high-temperature insulation material with a thermal conductivity of 0.79 W/(m·K) covering the copper block was included for minimizing the heat loss. Between the insulation and copper block was an air gap that also reduces conductive losses. The copper block was supported by four poor thermal conducting ceramic rods. A steel foil was covered on the inner wall of insulation layer for reducing heat loss by radiation.

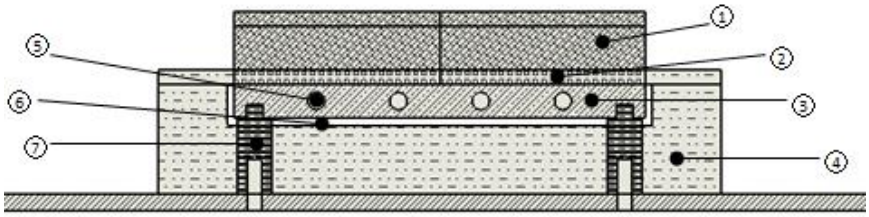

Figure 5-2 Test stand configuration (1) Water block, (2) TEGs, (3) Copper Block, (4) High temperature insulation layer, (5) Cartridge heater, (6) Air gap, (7) Ceramic rod [10]

5.2 Laboratory-based Testing

A laboratory-based test had been made for simulating the result of field installation. The adaptor, Hi-Z 2, and heat sink were installed on a section of 12 in. nominal size schedule 40 pipe provided by Calpine Power Plant at Stony Brook University. A schedule 40 pipe has a slightly larger inner diameter than the schedule 80 pipe, but the result would be similar since both of them have a negligible thermal resistance. The heat source was two curve face ceramic radiant heaters (Figure 5-3) which can provide 1300 W of heat. Figure 5-4 illustrates the ceramic radiant heaters installing inside a schedule 40 12 in. pipe.

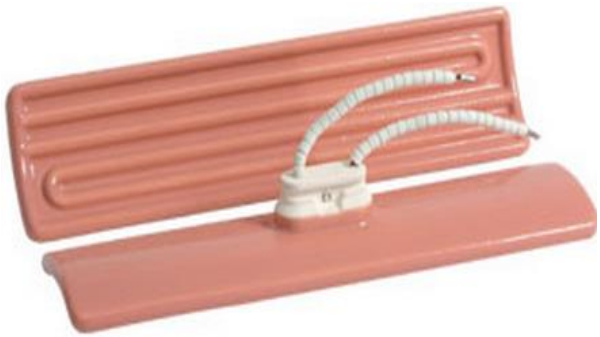

Figure 5-3 Ceramic radiant heaters [32]

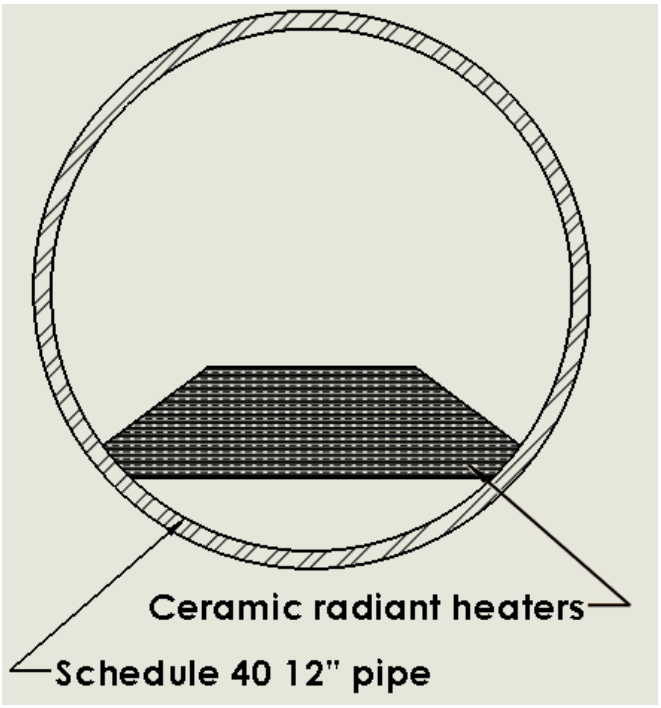

Figure 5-4 Ceramic radiant heaters inside the schedule 40 12 in. pipe

In order to make sure the material of the ceramic radiant heater can tolerate the temperature required to heat up the inner pipe wall, Equation 26 is applied to calculate the required temperature of the ceramic radiant heater, where σ is the StefanBoltzmann constant, T_h and T_w are temperature of heaters and inner pipe wall, A_h and A_w are the surface area of heater and inner pipe wall, F_{12} is the view factor of heater surface to pipe wall, and ε_h and ε_w are the emissivity of the heater surface and inner pipe wall [31].

$$\boldsymbol{Q} = \frac{\boldsymbol{\sigma}(\boldsymbol{T_h}^{\boldsymbol{4}} - \boldsymbol{T_w}^{\boldsymbol{4}})}{\left(\frac{\boldsymbol{1-\varepsilon_h}}{\boldsymbol{\varepsilon_h A_h}}\right) + \left(\frac{\boldsymbol{1}}{\boldsymbol{A_h F_{12}}}\right) + \left(\frac{\boldsymbol{1-\varepsilon_w}}{\boldsymbol{\varepsilon_w A_w}}\right)} \qquad (26)$$

The coarse surface of the schedule 40 pipe would create a large thermal contact resistance, therefore a graphite foil was placed between coupler and pipe in order to reduce the contacting gap due to surface roughness. Thermal couplers were attached on the pipe wall, heat conducting plate, and

heat sink for measuring pipe wall, TEG hot side, and TEG cold side temperatures. The left hand side of Figure 5-5 shows the configuration without fiber glass insulation layer. As one can see, the adaptor was clamped by two stainless steel Hose-clamp-style straps, and the sleeve of connecting rod was tighten by a pipe clamp. The schedule 40 pipe was wrapped by a fiber glass insulation layer and covered by a mineral wool insulation layer on the top in order to minimize the heat loss from convection (right hand side of Figure 5-5).

Figure 5-5 Testing setup without insulation layer (left) and testing setup with insulation layer (right)

Mounting of TEGs was very important in this experiment. Mounting without enough compression force would reduce the power output. Excessive or inequality of compression force would damage TEGs. TEG mounting method was based on the installation guide from Custom Thermoelectric [33]. The screw positions for TEG mounting should be between 0.5 mm and 12.7 mm from the sides of the TEG. A diagonal position is not allowed. Several examples of mounting configuration for mounting 4 TEGs are shown in Figure 5-6.

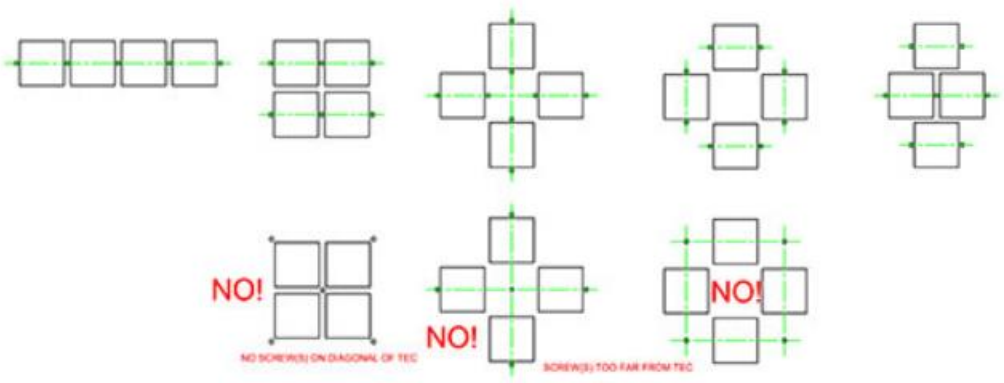

Figure 5-6 Examples of mounting configuration [33]

5.3 Field-based Testing

This test was made to verify the function of wireless network and sensing system. The location was at Calpine Power Plant at Stony Brook University since it is impossible to access SMRs in current stage.

As mentioned in 4.2, the selected steam pipe is 12 in. nominal size schedule 80 pipe which has an inner diameter 11.38 in. of and outer diameter of 12.75 in.. The steam was around 300 ºC and 4000kPa with a mass flow rate of 7.56 kg/s in winter (change during seasons).

The power plant was shut down for annual maintenance, therefore the pipe wall temperature was low enough for installation. The 2 in. insulation layer was also temporary took off for the convenience of installation. Four Hi-Z 2 were used in this test. The adaptor designed in section 4 including a 0.5 in. thick coupler with an arc angle of 105º, a 5 in. long connecting rod with a diameter of 1.5 in., and a 5 in. by 5 in. heat conducting plate with a thickness of 0.5 in.. Hose-clamp-style straps were used for attaching the design on steam pipe wall. Finally, the heat sink by HS Martson with thermal resistance of 0.28 was used as the cooling solution. Two thermal couples are attached on pipe wall and hot side of TEG. Figure 5-7 shows the entire design installed on the steam pipe.

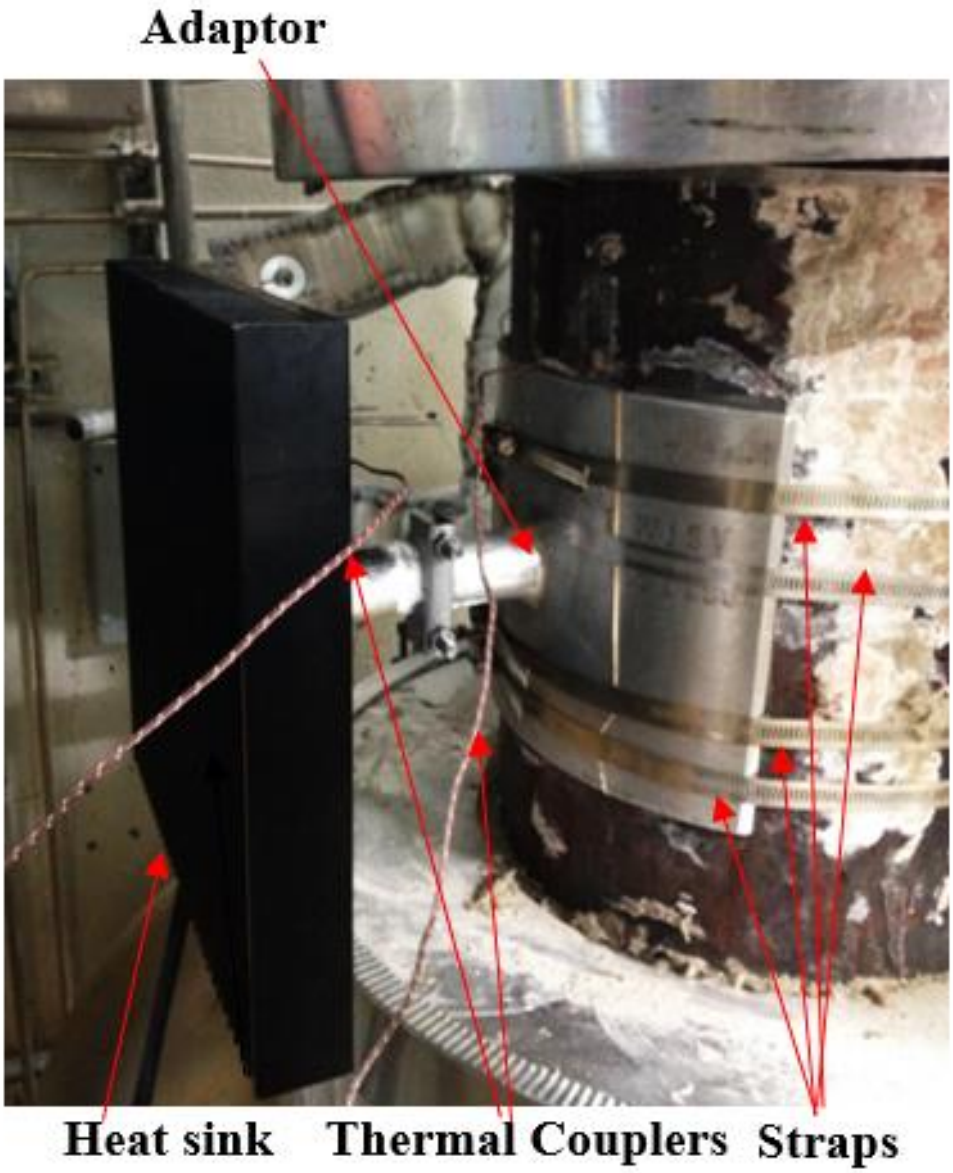

Figure 5-7 Entire design installed on the steam pipe

6 Results and Discussion

6.1 Nuclear Plant Operating Estimates

The selected installation sites are steam pipe housings in primary or secondary loop. The temperature of these locations ranges from 300 °C to 500 °C depends on the reactor type and location.

The ambient temperature near steam pipes is generally 35 °C in summer and 20 °C in winter. Gamma radiation, as mentioned in 2.3, is around 5×10^{-2} Gy/h in the coolant loop, while nuetron radiation is negligible.

These environmental conditions are identical to conditions in the field-based test except radiation involved. As one can see in Figure 6-1, heat is conducted by the adaptor which was designed for conducting adequate amount of heat to TEGs. The adaptor is attached on steam pipe by using pipe straps. Different natural convection heat sinks will be used under different boundary conditions. The electronics package with a wireless transceiver, power storage system, power management, and environmental protection enclosure will be attached on the heat sink. Several sensors such thermal couple, flowmeters, and radiation sensors are applied.

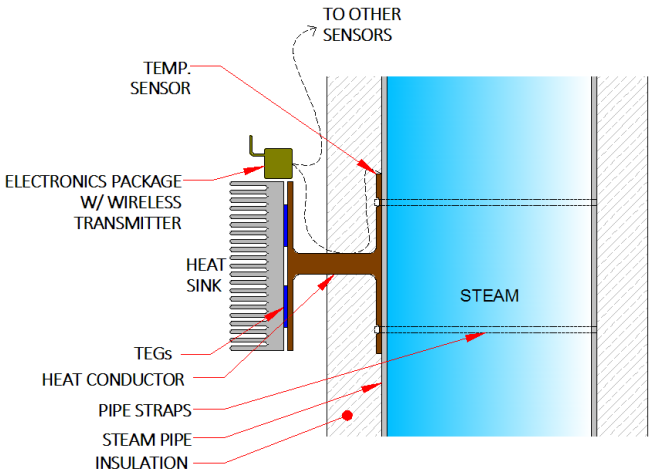

Figure 6-1 Cross section of prototype in nuclear power plants [34]

6.2 Thermal Analysis Results and Final Thermal Design

Knowing that the ideal temperature difference between TEGs is 100 °C, a 163.4 W of heat will be needed to apply on TEGs (obtained by Equation 5). Furthermore, total thermal resistance of the entire deign should not be more than 1.78 K/W otherwise temperature difference between TEGs will be lower than 100 °C because the temperature difference of the entire system is 290 °C.

In this design, the thermal contact area of coupler and heat conducting plate are relatively large in order to have better conducting efficiency. As a result, the thermal resistance of these two parts are expected to be negligible. Take coupler for example. Thermal resistances in different sizes are all so small that can be neglected (Table 6-1).

Table 6-1 Thermal resistances of couplers in different sizes

Thickness (in.)	Length (in.)	Arc angle (degree)	Thermal resistance (K/W)
0.5	6	60	1.4×10^{-3}
0.5	8	105	6×10^{-4}
0.75	6	60	2×10^{-3}
0.75	8	105	8.9×10^{-4}

Then, geometries were simply decided by the difficulty of machining and available size of raw material. The selected dimensions of coupler and heat conducting plate are shown below (Figure 6-2).

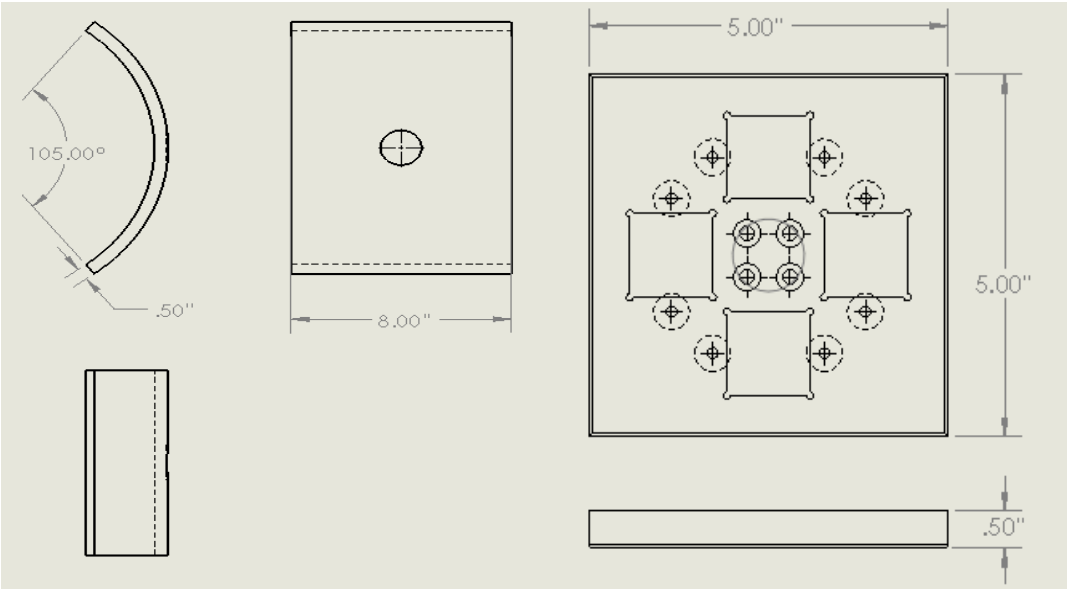

Figure 6-2 Dimensions of coupler and heat conducting plate

The heat transfer coefficient for superheated water determined by Equation 10 and Equation 12 is 254 $W/m^2 \cdot K$. Therefore, the thermal resistance of superheated water is also very small since the large surface area and high heat transfer coefficient. Thermal resistances of pipe wall, coupler, and heat conducting plate are 1×10^{-3}, 6×10^{-4}, and 4.5×10^{-3} K/W, respectively.

The connecting rod effects total thermal resistance the most because of its comparatively long length and small contact area. Its length is also fixed at 5 in. because of the thickness insulation layer of steam pipe. As a result, diameter became the only variable to adjust the total thermal resistance. Notice that thermal resistance of the heat sink thus should be lower than 0.306 K/W to maintain temperature of heat sink below 80°C (discuss in section 6.2.1). The 1.5 in. and 1.375 diameter rod are available raw metal sizes that make total thermal resistance of entire design close to 1.78 K/W. Thermal resistances of connecting rod with different diameters are shown in Table 6-2. The 1.5 in. rod are selected instead of 1.3745 in. rod, even though 1.5 in. one is closer to our requirement. The reason is that the real total thermal resistance would be higher than 1.78 K/W because this analysis didn't take thermal contact resistances between contacting surfaces into account.

Table 6-2 Thermal resistance of connecting rod and entire design with different rod diameters

Diameter (in.)	Thermal resistance of connecting rod (K/W)	Total thermal resistance (K/W)
1.375	0.77	1.79
1.5	0.65	1.67

6.2.1 Heat Sink Design

The goal of this heat sink design is to dissipate 163.4 W of heat and ensure temperature on heat sink is below 80 °C since electronic devices and wires might be attached on it in the field-based test. The thermal resistance of the heat sink thus should be lower than 0.306 K/W. By applying empirical equations, we can find the configuration for optimum performance. In this work, it was assumed that the available space for installing a heat sink is 0.15 m × 0.15 m × 0.28 m. As a result, the fin based area is fixed at 0.15 m × 0.15 m, while fin height (H) ranges from 0.2 m to 0.28 m

and fin thickness (t) ranges from 2 mm to 6 mm. The optimum fin spacing is already determined by Equation 13. The result of heat dissipation and thermal resistance by using empirical correlation equation are shown in Figure 6-3 and Figure 6-4, respectively. The red dash lines in these figures indicate required performance.

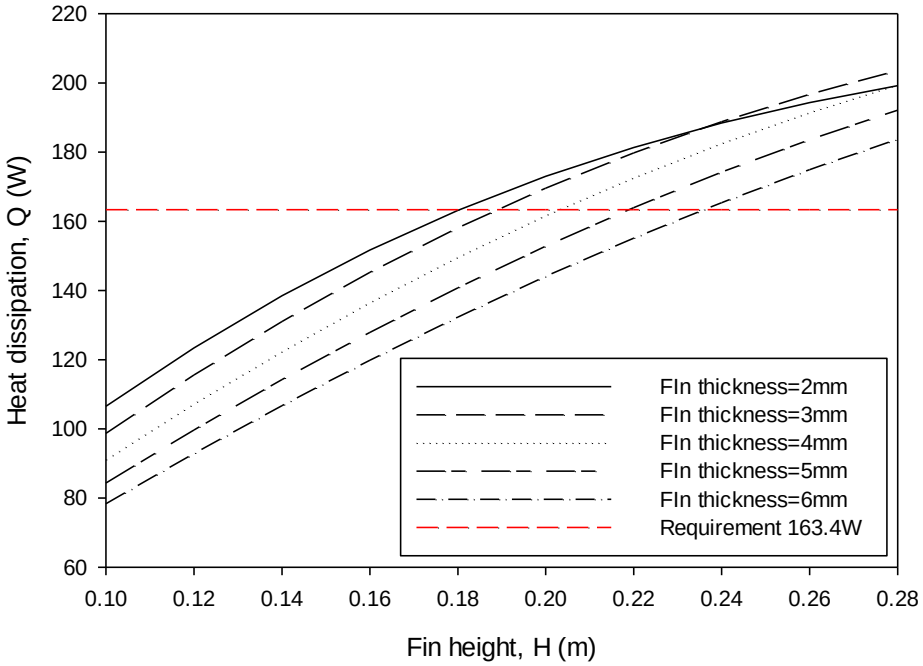

Figure 6-3 Heat dissipation varies with fin height under different fin thickness

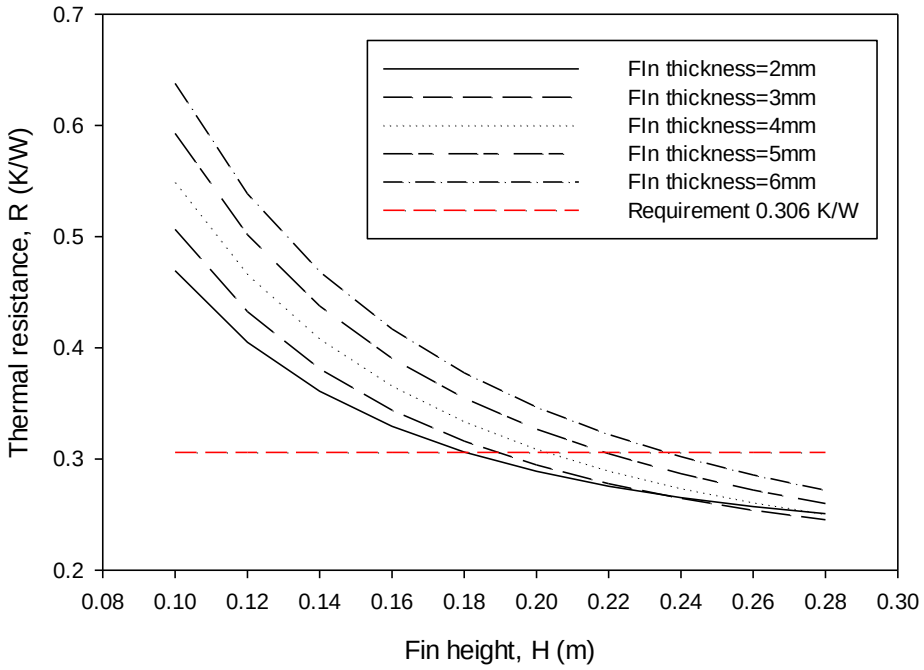

Figure 6-4 Thermal resistance varies with fin height under different fin thickness

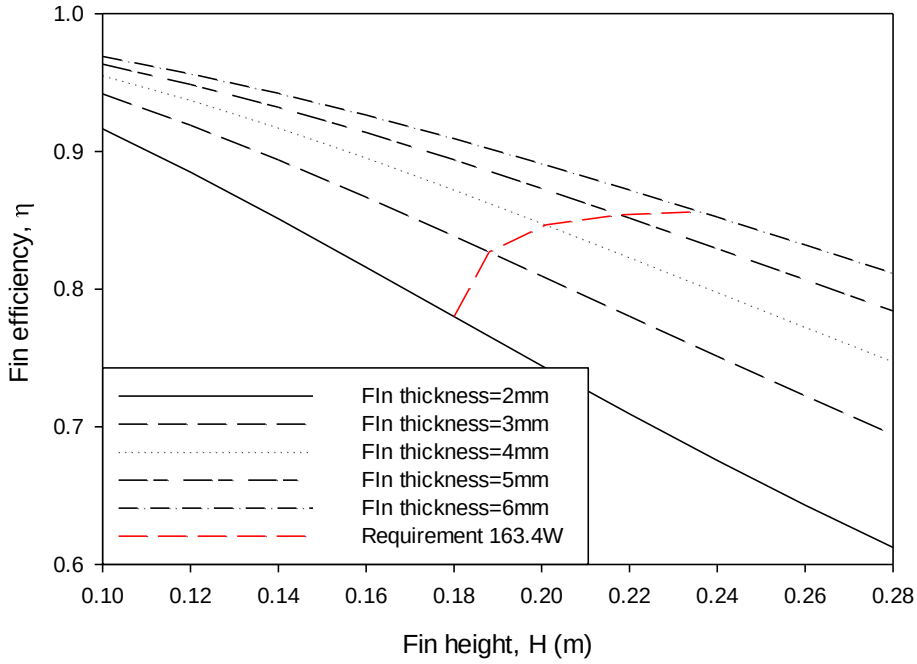

Figure 6-5 Fin efficiency varies with fin height under different fin thickness

As we can see heat sink with fin thickness 2 mm, 3 mm, 4 mm, 5 mm, 6 mm can satisfy the requirement after fin height higher than 0.18 m, 0.185 m, 0.2 m, 0.22 m, and 0.24 m, approximately. To determine the best heat sink configuration, the fin efficiency is also a very important factor. A smaller heat sink with higher fin efficiency might be comparable to a larger heat sink with low fin efficiency. As shown in Figure 6-5, thicker and shorter fins leads to higher fin efficiency. The heat sink with 6 mm fin thickness and 0.24 m fin height, which has a thermal resistance of 0.302 K/W and is able to dissipate 165.5W of heat, can satisfy our requirement and also has a high fin efficiency (86%) is an ideal heat sink configuration.

The result of CAE simulation made for confirming the analytical analysis is shown below.

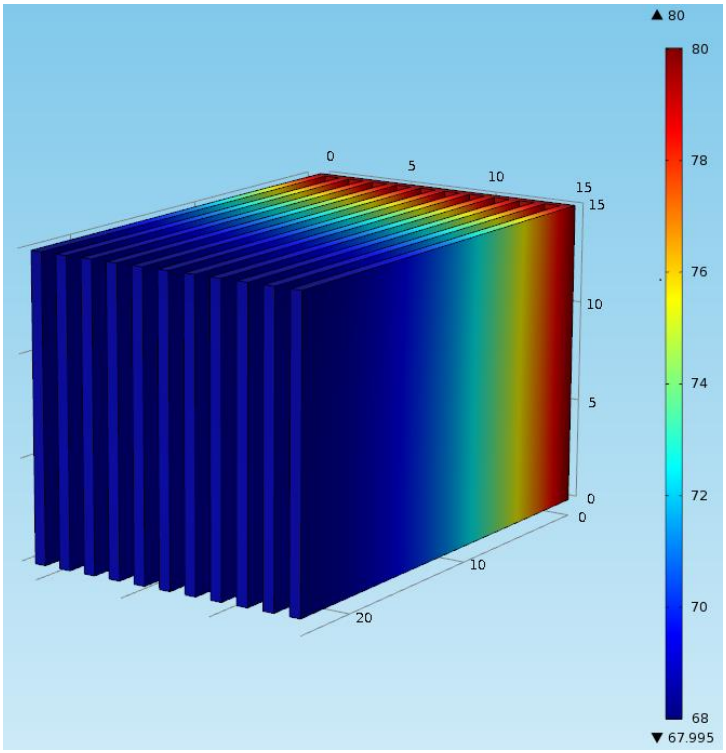

Figure 6-6 Temperature distribution on customized heat sink

Figure 6-6 shows the temperature distribution on this customized heat sink. According to the result, this heat sink can dissipate 170.65 W. By the definition of thermal resistance (Equation 5),

the thermal resistance of this customized heat sink is 0.293 K/W, which is better than the analytical result. The reason is that the analytical result only takes convection on vertical walls into account since it is based on correlation equation for vertical walls only, while CAE analysis consider convection on both vertical and horizontal walls.

Unfortunately, making a customized heat sink is time consuming and expensive in current situation. We decided to buy a commercial product which also matches the requirement. Figure 6-7 is the technical data sheet provided by HS Martson. According to this data sheet, this heat sink has a thermal resistance of 0.29 K/W when the length reaches 250 mm. The one we bought is 300 mm long with a thermal resistance of 0.28 K/W. However, HS Martson 96CN-03000-A-200 has a relatively large base area and shorter fin height. A customized heat sink will allow for more design flexibility based on space available at different target locations.

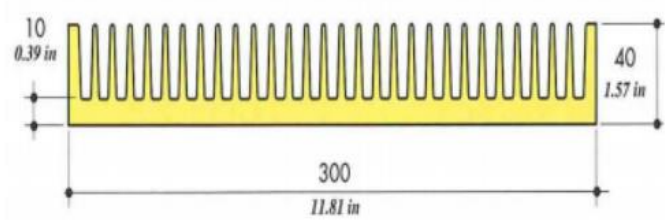

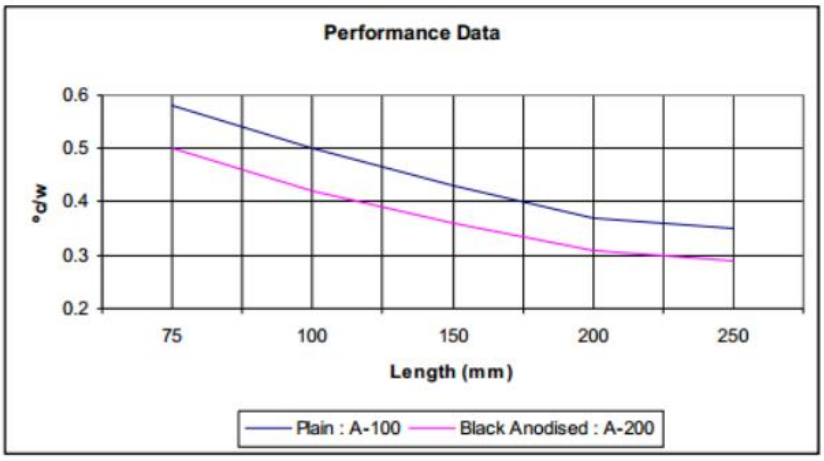

Figure 6-7 Technical data sheet of HS Martson 96CN-03000-A-200 [22]

The result of CAE simulation made for verifying the performance claimed by the manufacturer is shown as Figure 6-8.

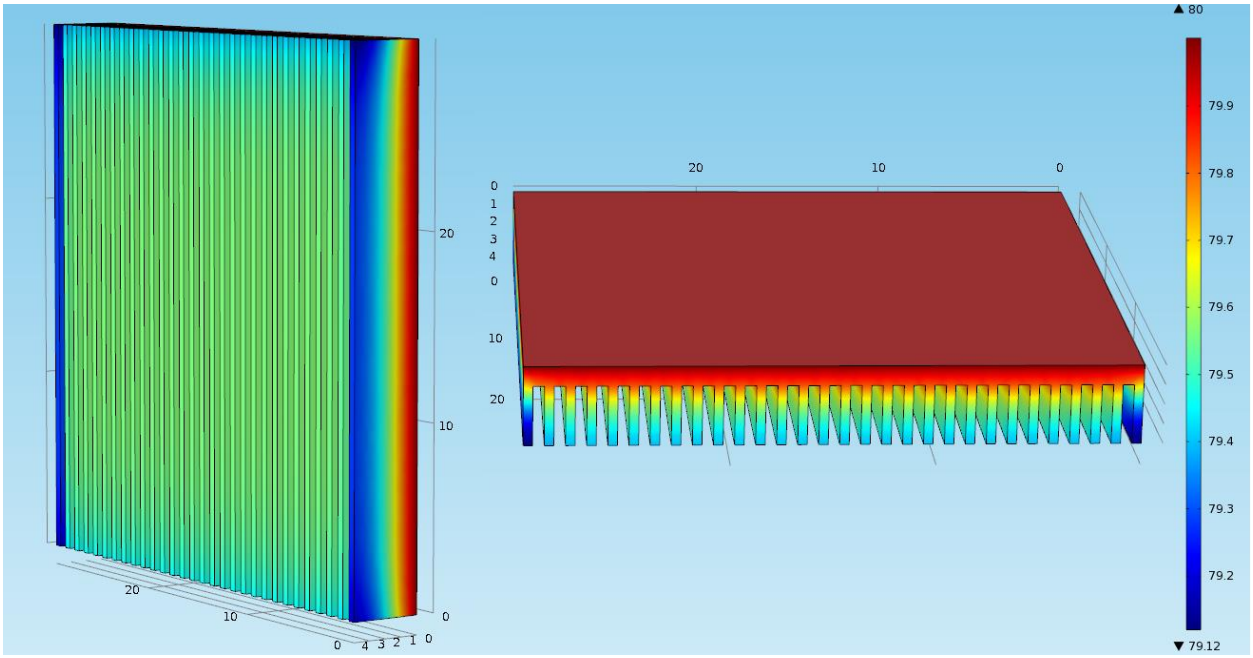

Figure 6-8 Temperature distribution on HS Martson 96CN-03000-A-200

This result is based on constant temperature boundary condition. The heat dissipated by convection on vertical walls, convection on horizontal walls, and radiation effect are 127.9 W, 7.05 W, 39.5 W, respectively. The thermal resistance of this heat sink is 0.287 which is very close to the performance they claims.

6.2.2 Thermal Design

Finally, the entire system including steam pipe, coupler, connecting rod, heat conducting plate, TEGs, and heat sink was simulated. Figure 6-9 is the temperature distribution of the entire system. The average temperature at different locations are shown in Table 6-3.

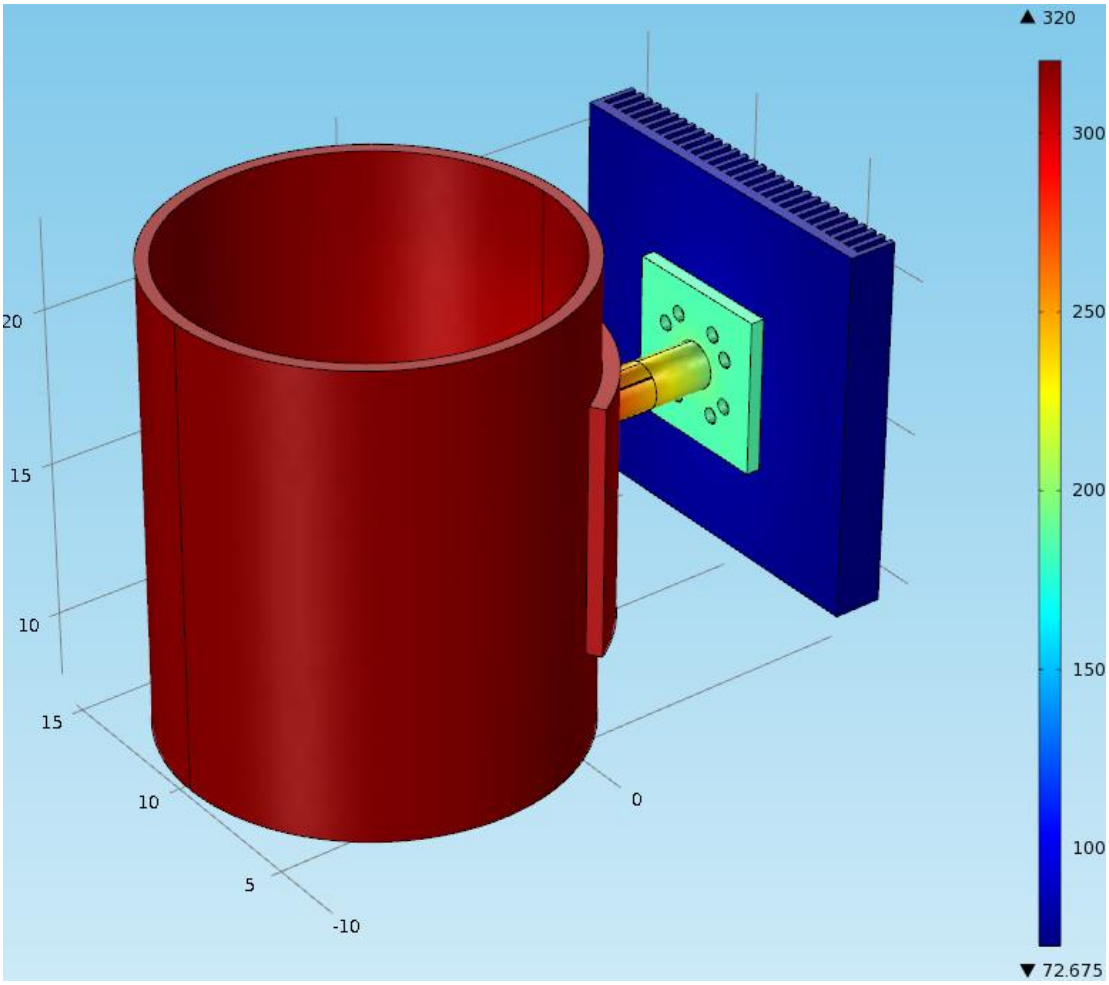

Figure 6-9 Temperature distribution of entire system

Table 6-3 Temperature at different locations of entire design (simulation based result)

Locations	Surface Temperature (ºC)
Pipe Wall	319
Coupler	312.2
Heat Conducting Plate (bottom)	188
Heat Conducting Plate (top)	186.3
Heat Sink (bottom side)	77.1

As one can see in Figure 6-10, the temperature on the hot side and the cold side of TEG are 189.57 ºC and 83.15 ºC. Therefore a 106.42 ºC of TEGs temperature difference is expected to be seen in this design which is very close to 100 ºC.

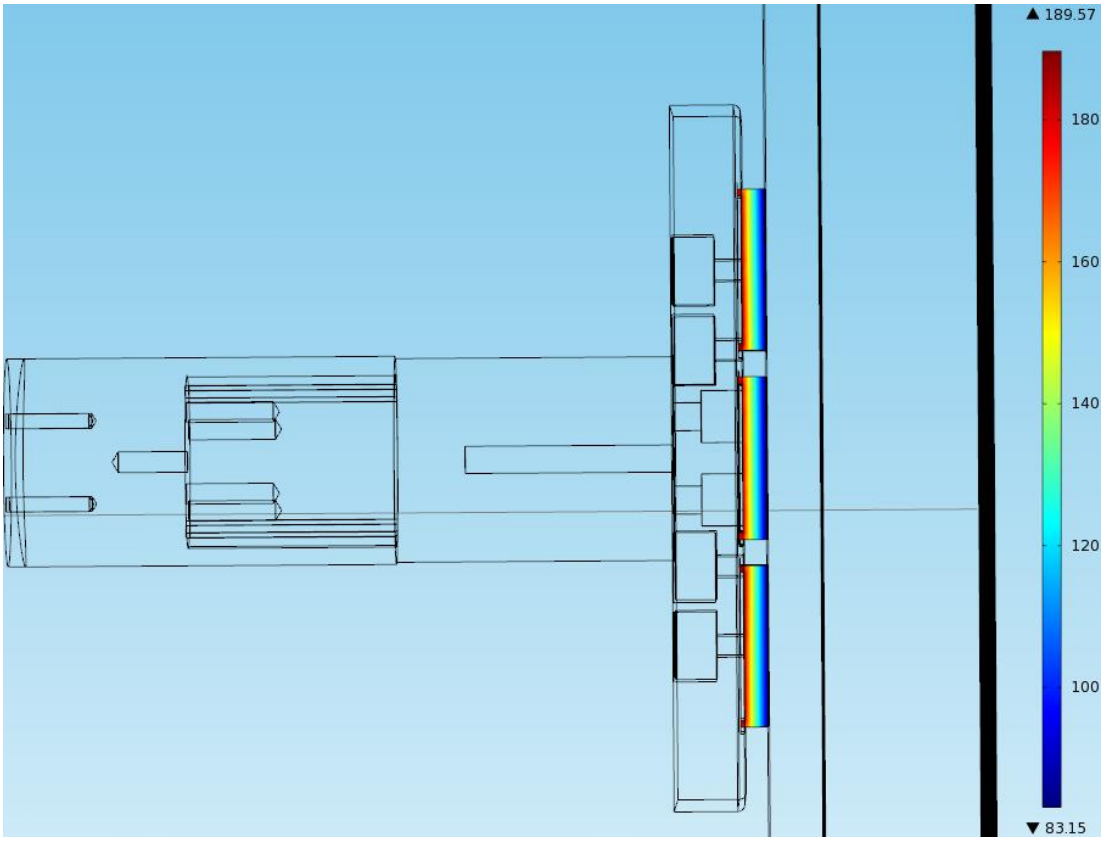

Figure 6-10 Temperature drop on TEGs

6.2.3 Thermal Expansion

Thermal expansion is the tendency of matter to increase or decrease in volume in response to temperature change. The expansion of pipe wall and coupler will affect the thermal contact resistance. A gap will appear in the mid of coupler if the pipe wall expands more than coupler. In contrast, contact area will only appear in the mid of coupler if the pipe wall expands more than coupler. Either these two scenarios will increase the thermal contact resistance significantly.

The Aluminum 6061 made coupler has a thermal expansion coefficient of 23.5 m/m K.

The steam pipe is made by AISI 1018 which has a thermal expansion coefficient of 12.06 m/m K.

Figure 6-11 shows coupler after thermal expansion with a scale factor of 10 while color bar indicates the displacement in Y direction (in inches).. Figure 6-12 shows steam pipe after thermal expansion with a scale factor of 10 while color bar indicates the displacement in X direction (in inches). Figure 6-13 shows the gap when two parts are attached without extra force applied.

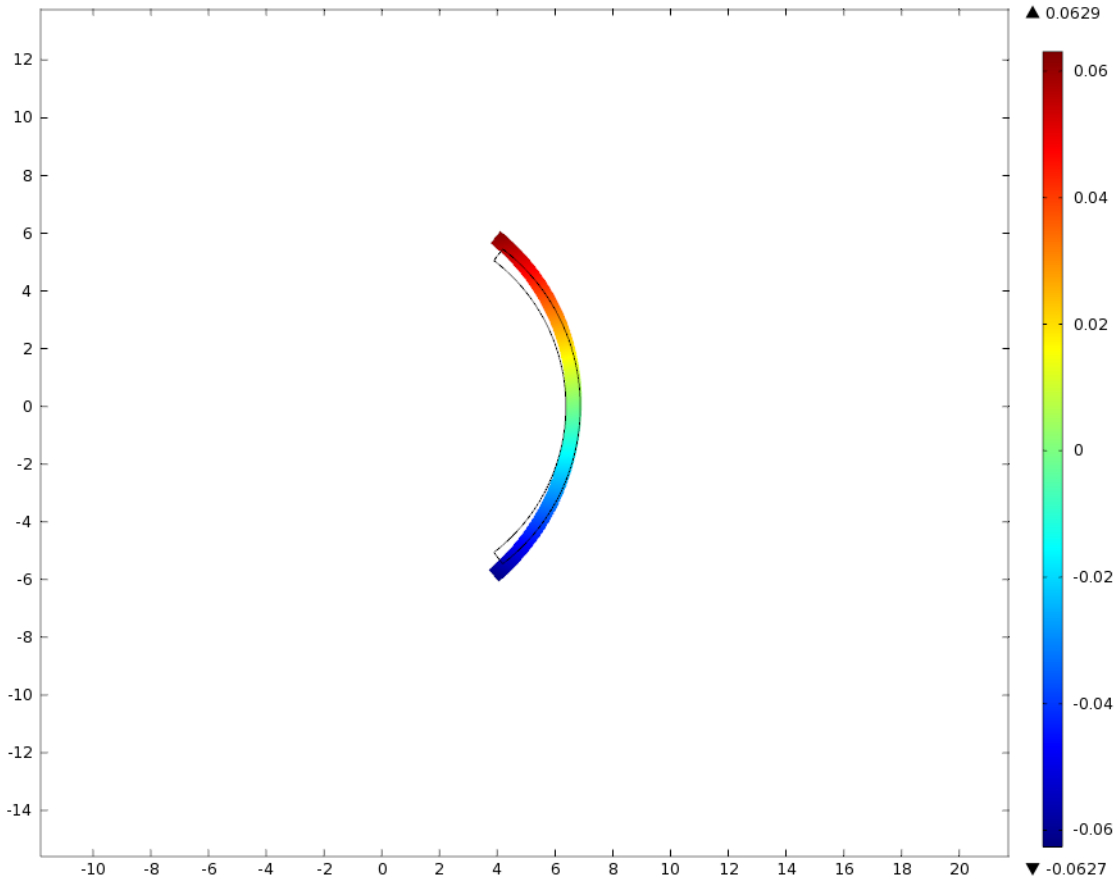

Figure 6-11 Thermal expansion of coupler in Y direction

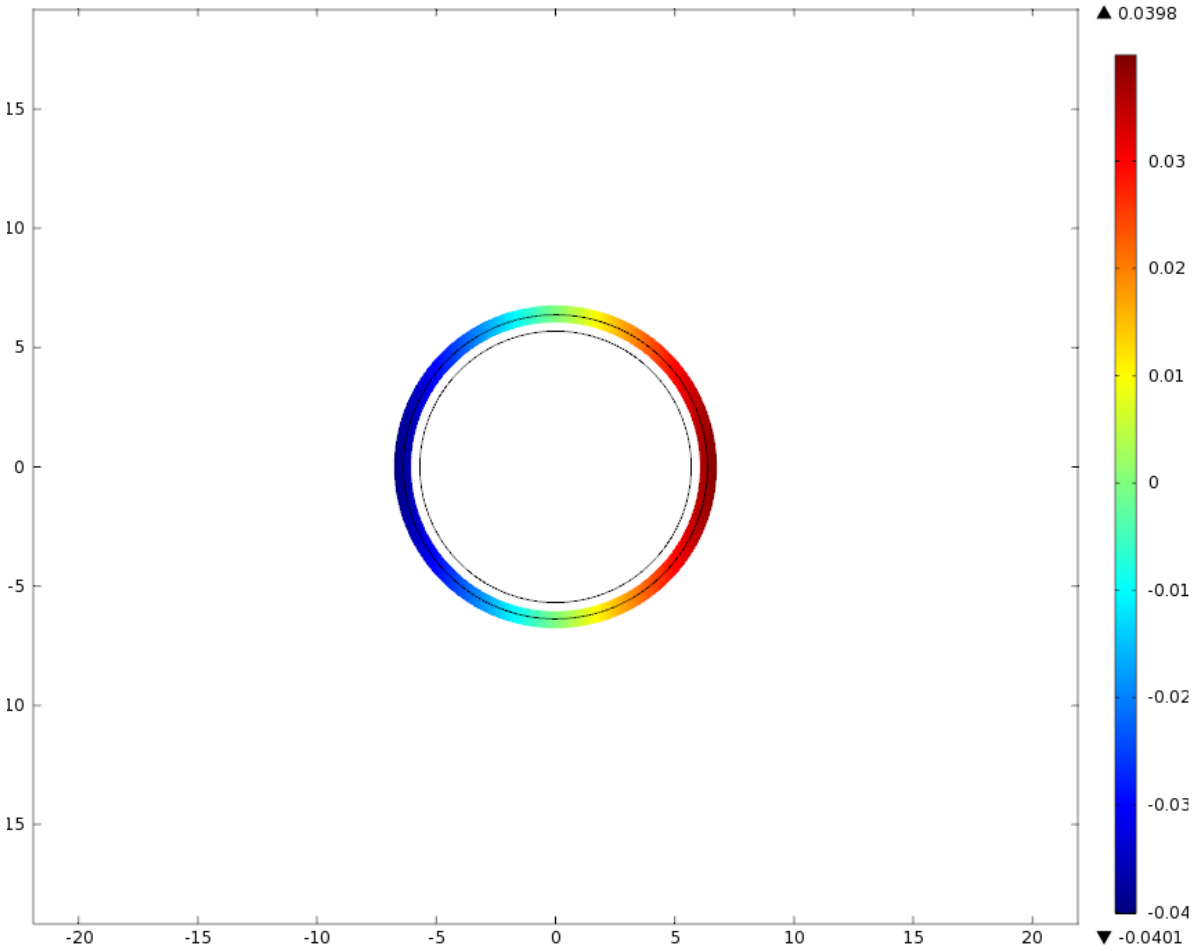

Figure 6-12 Thermal expansion of steam pipe in X direction

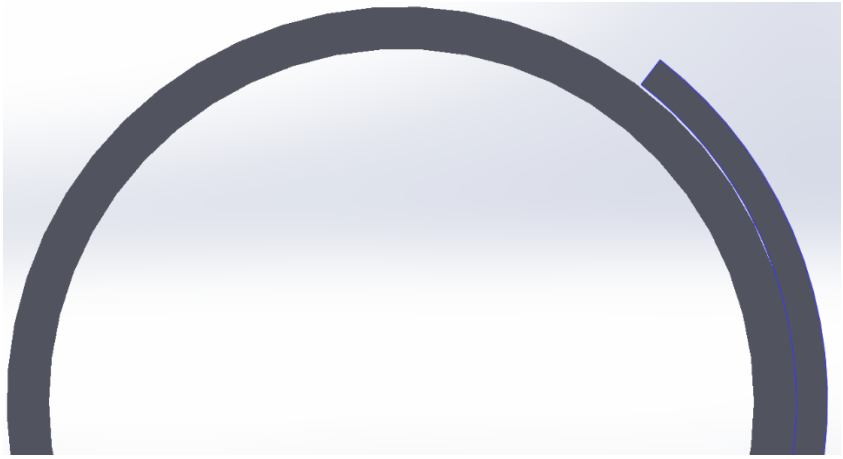

Figure 6-13 Gap between coupler and steam pipe after thermal expansion

This result indicates the maximum gap between parts is 0.04 in. which can be filled by graphite foil. Also, the mechanical attachment (will be introduced in the next section) can apply enough force for bending the coupler and thus minimize the gap.

6.3 TEG Testing Results

The first test (Figure 6-14) tested the Hi-Z 2 which is claimed can produce 2.5 Watts and 3.3 Volts at matched load when there is a 200°C temperature difference. The hot side temperature was fixed at 230 °C by a temperature controller. The cold side temperature, however, was not as stable as hot side ranged from 43.5 °C to 54.9 °C. The Hi-Z 2 available at that time was a downgraded version which only generates 80% of power claimed in the data sheet. Therefore, the W^*_{ideal} in Table 6-4 are calculated as 80% of Hi-Z 2 theoretical power output. The best result of power generation is 78% of the ideal power output. An inappropriate compression method which causes the inequality of torque applied on two screws could lead to the damage of TEG or poor thermal contact.

Table 6-4 Result of the first test

	T_h (°C)	T_c(°C)	V_{max}	W_{max}	W^*_{ideal}	W_{max}/ W^*_{ideal}
TEG 1	230	43.5	2.35	1.5	2.248	0.67
	230	54.2	2.31	1.4	1.786	0.78
TEG 2	230	54.9	2.39	1.319	1.96	0.67
	230	50.2	2.25	1.321	2.08	0.64

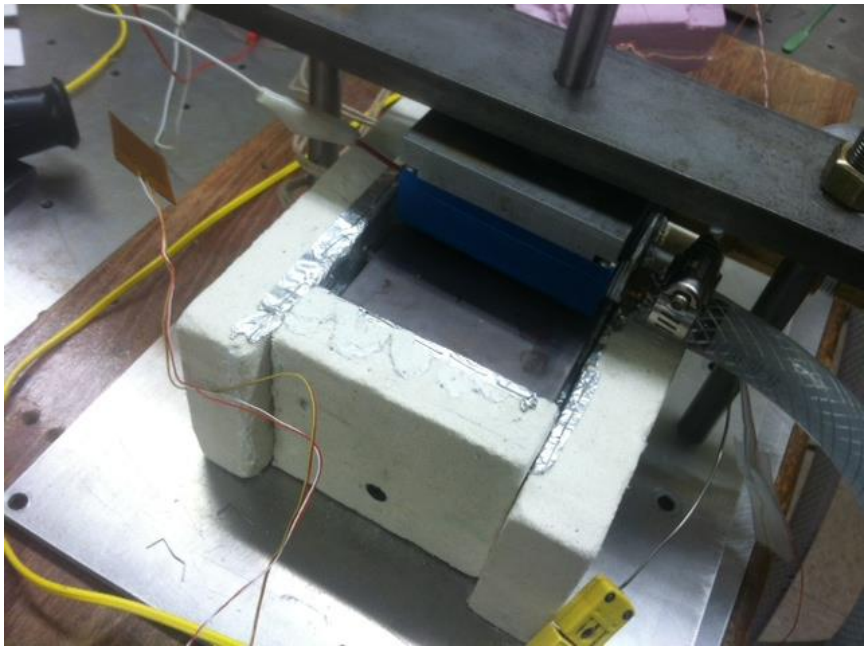

Figure 6-14 Setup of the first test

In the second test (Figure 6-15), Hi-Z 2 was replaced by the 1263-4.3 from TECTEG. A modified compression method was also applied. A torque wrench is used for optimizing compression force (minimum 7.5in-lbs per screw). Two 1263-4.3 from TECTEG were tested independently in this test. The hot side temperature in this test is fixed at 250 °C. As shown in Figure 6-16, the ideal open circuit voltage and matched load power when hot side and cold side are 250 °C and 50 °C are approximately 7.8 V and 3 W. Referring to Table 6-5, the result of TEG 2 is very close to the data sheet (85%).

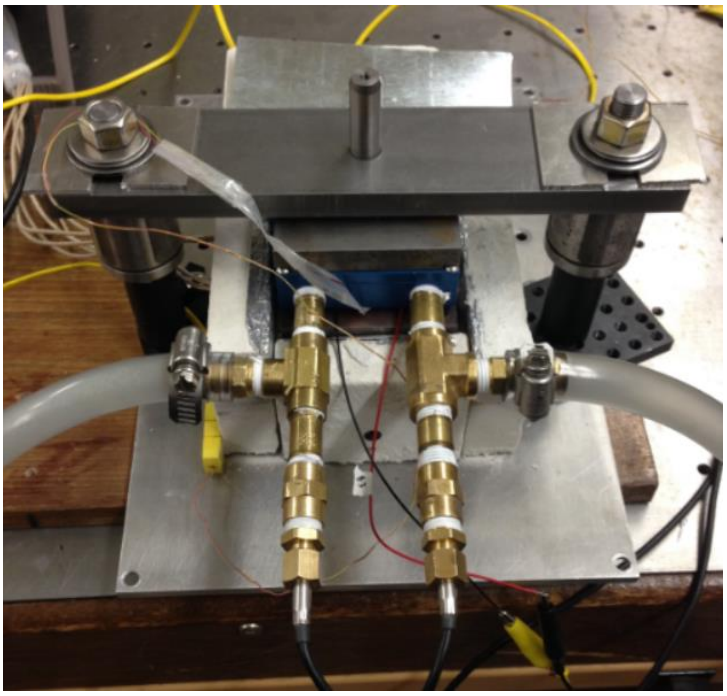

Figure 6-15 Setup of the second test

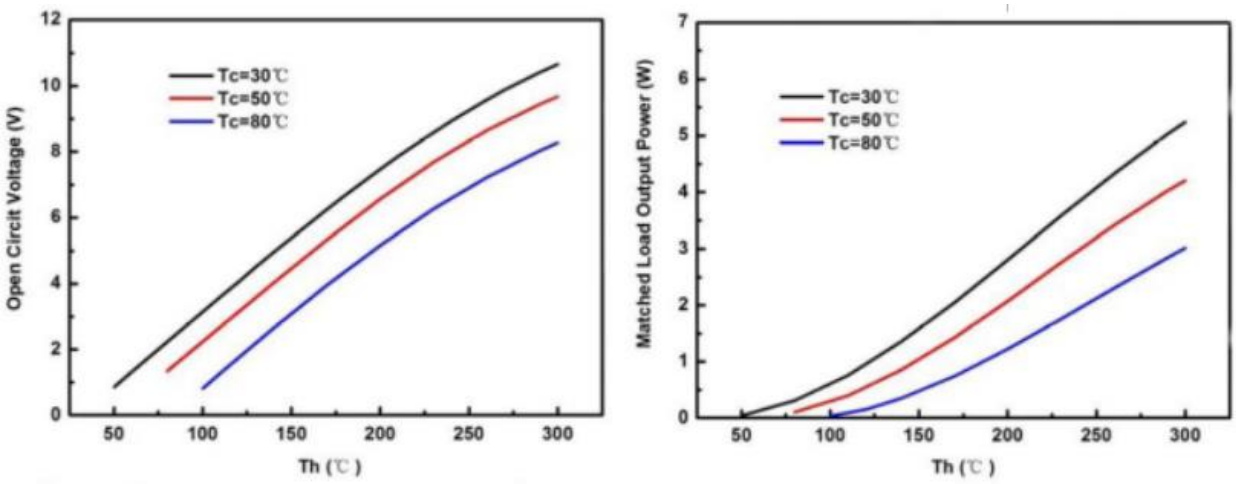

Figure 6-16 Technical data sheet of 1263-4.3 from TECTEG [20]

Table 6-5 Results of the second test

	T_h (°C)	T_c(°C)	V_{max}	W_{max}	$W^*_{@\ Tc=50\ °C}$	$W_{max}/\ W^*_{@\ Tc=50\ °C}$

TEG 1	250	42.4	7.2	1.915	3	0.64
TEG 2	250	42.4	7.83	2.438	3	0.85

6.4 Lab-based Testing Results

To provide 163.4 W of heat to the adaptor and maintain the temperature of the pipe wall at 250 ˚C, the temperature of the ceramic radiant heats will need to heat up to 492 ˚C, while the ceramic heater allows temperatures of over 1600 ˚C and its aluminized steel shell can maintain strength at temperatures up to 677 °C. By the time of this experiment, the1263-4.3 from TECTEG was not available, therefore, Hi-Z 2 was used in this experiment. Four Hi-Z 2 can provide enough power to satisfy the power requirement for electronic devices. A better mounting method was applied based on the installation guide from Custom Thermoelectric. A comparison between actual testing result and estimated result is shown in Table 6-5. Temperature at pipe wall was fixed by the temperature controller at 250 ˚C, 260 ˚C, and 280˚C.

Table 6-6 Lab-based testing results (four TEGs)

Pipe wall temperature (˚C)	250		260		280	
	Actual	Simulation	Actual	Simulation	Actual	Simulation
Hot side temperature (˚C)	110	136.6	114.4	141.7	137	152
Cold side temperature (˚C)	48.4	64	50.8	66	55.2	69.6
Estimated open circuit voltage under actual condition (V)	7.48×80% = 6		7.88×80% = 6.3		10.04×80% = 8.03	
Actual open circuit voltage under actual condition (V)	5.3		5.6		6.48	

The TEGs used in this test were also a downgraded version that only provides 80% of the performance claimed in the data sheet. As one can see, the actual open circuit voltage under actual condition is around 90% of the performance claimed by manufacturer (Table 6-6). Figure 6-17 indicates the temperature distribution under 250 ˚C of the pipe wall temperature, the actual temperature dropped 22.8 % more from pipe wall to the hot side of TEGs (from 0 in. to 6 in.) than estimation. This was affected by the heat loss from connecting rod surface and poor thermal contact between sleeve and rod. Temperature dropped 14 % less between TEGs (from 6 in. to 6.5 in.) than estimation. It was because less heat conducted to TEG because of heat loss from pipe wall to hot side and screws conducted additional heat to heat sink thus reduced the temperature difference.

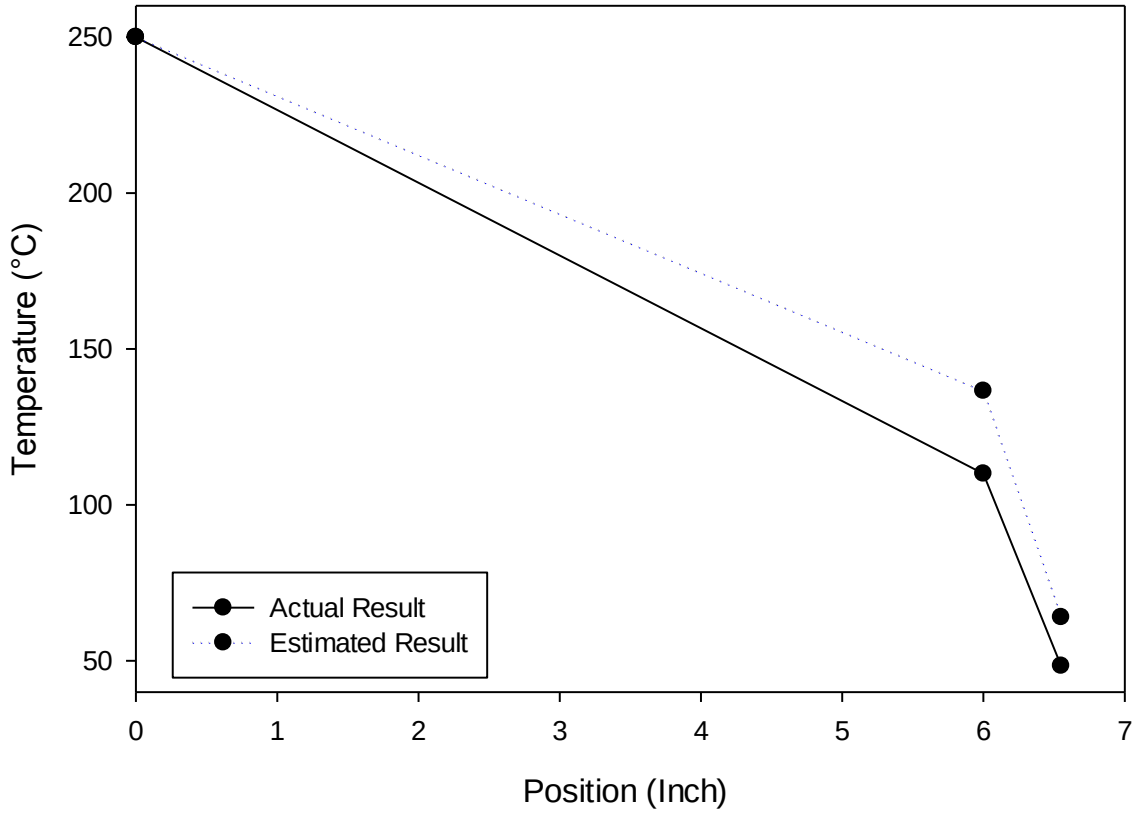

Figure 6-17 Lab-based testing results

Therefore, several modifications were made to improve the performance:

- An additional insulation layer for covering the connecting rod.
- Thermal grease applied on the contact surface between sleeve and rod.
- Adding Ceramic or other insulation washer to avoid heat conducted through screws.

.

6.5 Field-based Testing Results Campus Power Plant

A prototype of this TEG powered sensing system was tested in the Calpine Power Plant at Stony Brook. The whole system at work is shown in Figure 6-18. The circuit board with a plastic enclosure was attached on an electrical wire tube, and two thermocouples were connected to the circuit board for temperature measurements in this test. The natural convection heat sink installed vertically outside the insulation layer. The infrared picture (Figure 6-19) indicated the highest temperature of the heat sink (cold side of TEGs) was about 57 °C. The temperature of the pipe wall was about 300°C with a ±10°C fluctuation and temperature at the TEG mounting plate (hot side of TEGs) was about 140°C. Therefore the temperature difference of the TEGs was about 70°C -80°C. These results were lower than simulation result because of lower steam (300 °C) and ambient temperature (20 °C), and poor thermal contact surfaces.

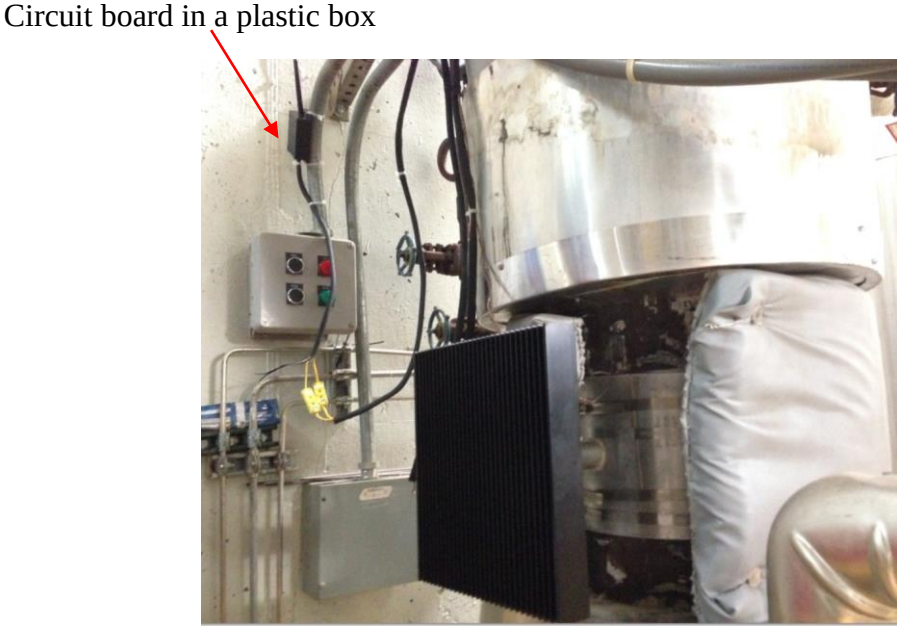

Figure 6-18 Entire system at work

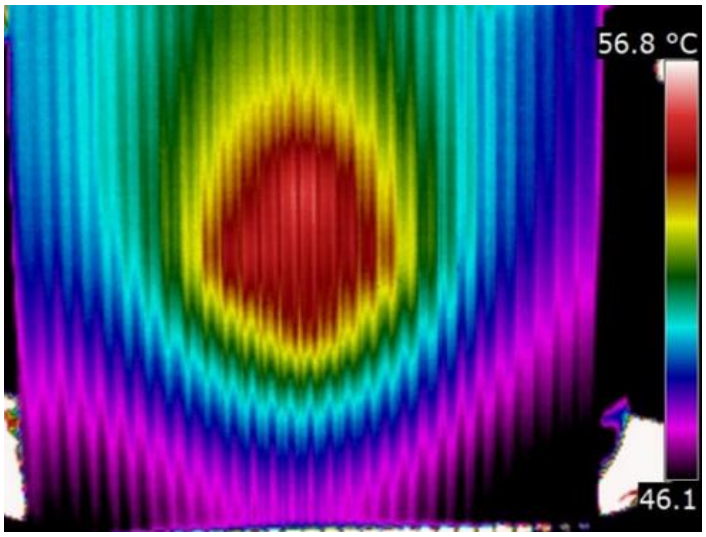

Figure 6-19 Infrared picture on heat sink

The open circuit voltage from four TEGs was about 9.32 V and the matched load voltage was 4.46 V while the circuit board was 3.37V. This result was 90% of the performance claimed by Hi-Z. Figure 6-20 shows the maximum power output was 1.3 Watts at 16 Ohms.

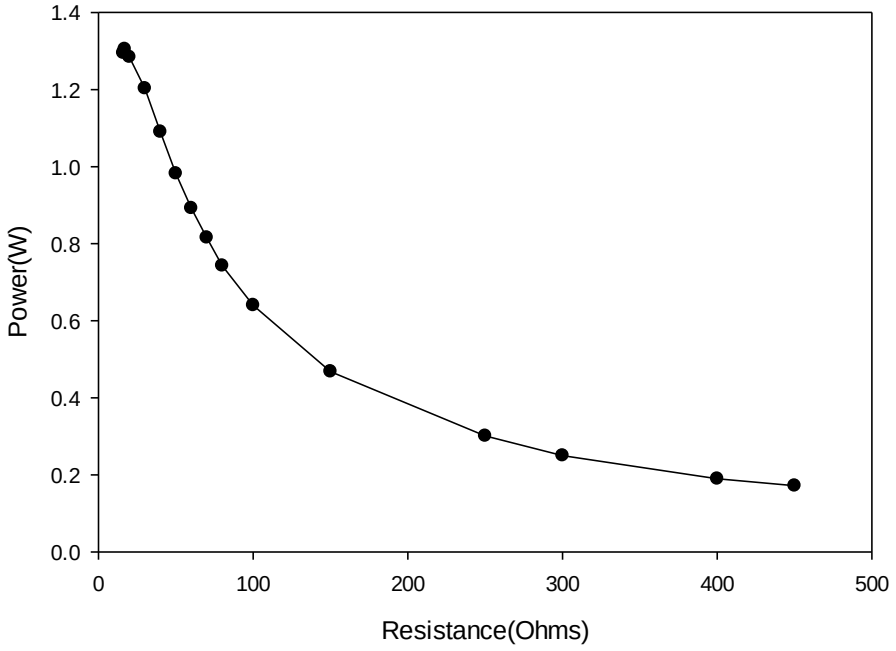

Figure 6-20 Power vs. Resistance

Figure 6.21 shows the hot side, pipe wall, circuit board temperature over 24 hours which were acquired by thermocouples and transmitted to offsite laptop wirelessly.

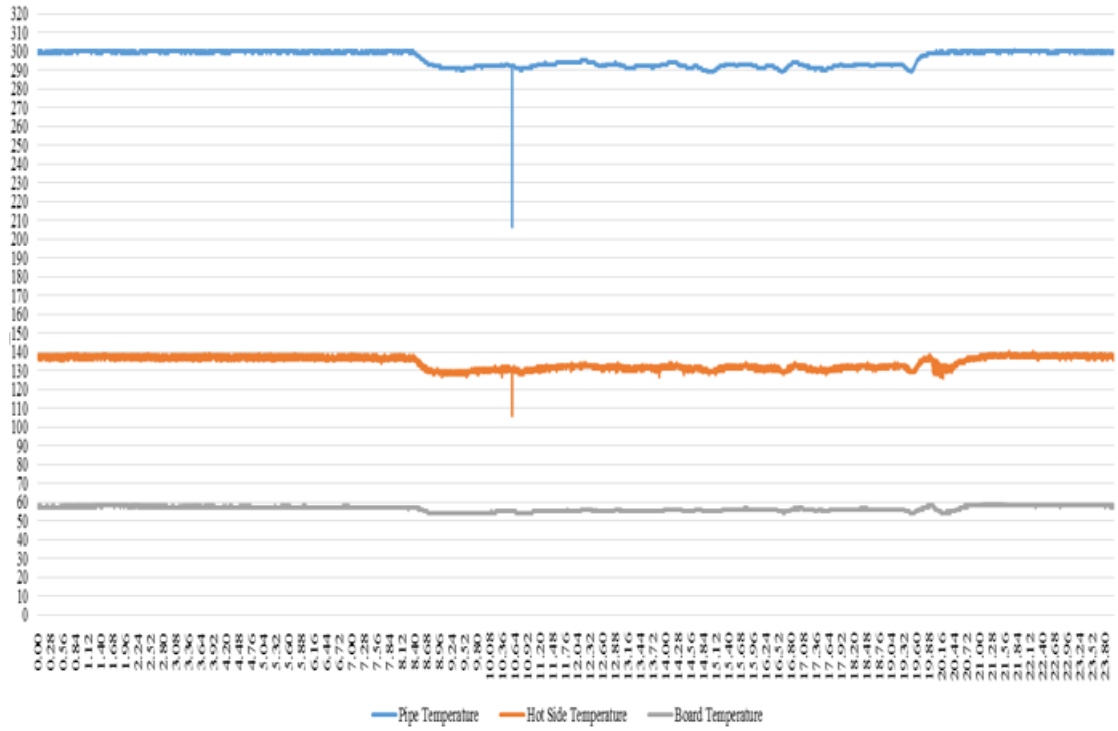

Figure 6-21 System temperature in 24 hours

7 Conclusions and Future Work

The loss of sensing ability in Nuclear power plant could cause an irreversible disaster. Therefore, a sensing system can function independently through generating power by TEGs has a very promising future. From the results above, it was proved that the entire design is feasible and reliable to work for a long time. The thermal design is very success which maintains the temperature at locations of interest in an ideal range.

The performances of selected TEGs were tested in a TEG test rig. The result indicated that a further study of TEGs compression method and thermal contact resistance are necessary in order to get a better TEGs performance. A laboratory-based testing was performed for proving the feasibility of

this design. Finally, the design including adaptor, TEGs, heat sink, temperature sensors, and wireless transmitter were tested in the field-based test. This design can provide a continuous and reliable source for obtaining data. A wireless transmitter which has a transmission range of 100 m was used for transmitting data to an on-site laptop, and the on-site laptop then uploaded the data through internet.

A 2nd generation device will be installed in the Stony Brook steam plant. The target location will be attached to an 8 in. horizontal steam pipe, which is 115°C, making the heat pipe technology feasible in this design. A radiation test for identifying the influence of radiation effects on electronic devices and TEGs is performing at this time. As for the features to endure harsh conditions, the environment protection enclosure designed in section 3.4 was not included in the field-based testing yet. Therefore, a detailed design, e.g. thickness of each layer, method of making a multiple-layer enclosure, and heat transfer problem inside the enclosure, will be discussed in the future.

References

[1] "Current Status, Technical Feasibility and Economics of Small Nuclear Reactors," Nuclear Energy Agency, Organisation for Economic Co-operation and Development2011.

[2] D. Fischer, *History of the International Atomic Energy Agency: the first forty years*: IAEA, 1997.

[3] S. Eide, *Reevaluation of station blackout risk at nuclear power plants*: Division of Risk Analysis and Applications, Office of Nuclear Regulatory Research, US Nuclear Regulatory Commission, 2005.

[4] P. Kuan, D. Hanson, and F. Odar, "Managing water addition to a degraded core," EG and G Idaho, Inc., Idaho Falls, ID (United States)1991.

[5] G. J. Snyder and T. S. Ursell, "Thermoelectric efficiency and compatibility," *Physical review letters*, vol. 91, p. 148301, 2003.

[6] D. Rowe and G. Min, "Design theory of thermoelectric modules for electrical power generation," *IEE Proceedings-Science, Measurement and Technology*, vol. 143, pp. 351-356, 1996.

[7] D. M. Rowe, *CRC handbook of thermoelectrics*: CRC press, 1995.

[8] A. F. Ioffe, *Semiconductor thermoelements and thermoelectric cooling*: Infosearch London, 1957.

[9] L. L. Baranowski, G. J. Snyder, and E. S. Toberer, "Concentrated solar thermoelectric generators," *Energy & Environmental Science*, vol. 5, pp. 9055-9067, 2012.

[10] U. S. D. o. Energy. (2014). *Small Modular Nuclear Reactors*. Available: http://energy.gov/ne/nuclear-reactor-technologies/small-modular-nuclear-reactors

[11] H. Spieler, "Introduction to radiation-resistant semiconductor devices and circuits," in *AIP Conference Proceedings*, 1997, pp. 23-49.

[12] H. C. Chih Chieh Lin, Mahder Tewolde, Gaosheng Fu, Di Liu, Tao Zhang, He Tao, Chao Nie, Weixiao Zheng, Fan Liu, Lei Zuo, David Hwang, Jon Longtin1, "Thermoelectrically Powered Sensing For Small Modular Reactors," in *ASME 2013 Summer Heat Transfer Conference*, Minneapolis, Minnesota, USA.

[13] L. P. Houssay, "Robotics and radiation hardening in the nuclear industry," University of Florida, 2000.

[14] G. R. Kilp and P. V. Mitchell, "RADIATION EFFECTS ON THERMOELECTRIC MATERIALS," WCAP-1680 United States10.2172/4790249Tue Feb 05 23:24:24 EST 2008DTIE; NSA-16-027696English, 1961.

[15] J. M. Harrer and J. G. Beckerley, "Nuclear power reactor instrumentation systems handbook. Volume 1," TID--25952-P1; ISBN--0-87079-005-6 United States10.2172/4480112Wed Dec 12 09:29:57 EST 2012Dep. NTISTIC; NSA-28-010208English, 1973.

[16] "Nuclear Reactor Types " The Institute of Engineering and Technology2008.

[17] *Advanced Reactors Information System*. Available: https://aris.iaea.org/sites/overview.html

[18] K. Bonsor. *How Black Boxes Work*. Available: http://science.howstuffworks.com/transport/flight/modern/black-box.htm

[19] *Hi-Z 14 and Hi-Z 2 from Hi-Z Technology*. Available: http://www.hi-z.com/

[20] *TEG1-1263-4.3 and TEG1-12610-5.1 from TECTEG*. Available: http://www.tecteg.com/modules.php?id=6
[21] *TG12-8-01L from II-VI Marlow designs and manufactures*. Available: http://www.marlow.com/products/power-generators/standard-generators/tg12-8-01l.html
[22] *1261G-7L31-05CQ from Custom Thermoelectric*. Available: http://www.customthermoelectric.com/powergen/pdf/1261G-7L31-05CQ_20140328_spec_sht.pdf
[23] S. Kakaç and Y. Yener, "Heat conduction," p. 56, 1993.
[24] A. P. Colburn, "A method of correlating forced convection heat-transfer data and a comparison with fluid friction," *International Journal of Heat and Mass Transfer*, vol. 7, pp. 1359-1384, 1964.
[25] A. Bejan, *Convection Heat Transfer*: Wiley, 2004.
[26] Y. A. Çengel and A. J. Ghajar, "Heat and mass transfer: fundamentals & applications," pp. 170-171, 488-495, 528, 535, 2011.
[27] A. Bar-Cohen and W. Rohsenow, "Thermally optimum spacing of vertical, natural convection cooled, parallel plates," *Journal of Heat Transfer*, vol. 106, pp. 116-123, 1984.
[28] R. Harper and W. B. Brown, *Mathematical equations for heat conduction in the fins of air-cooled engines*: National Advisory Committee for Aeronautics, 1923.
[29] S. W. Churchill and H. H. Chu, "Correlating equations for laminar and turbulent free convection from a vertical plate," *International journal of heat and mass transfer*, vol. 18, pp. 1323-1329, 1975.
[30] J. Lloyd and W. Moran, "Natural convection adjacent to horizontal surface of various planforms," *Journal of Heat Transfer*, vol. 96, pp. 443-447, 1974.
[31] F. P. Incropera, A. S. Lavine, and D. P. DeWitt, *Fundamentals of heat and mass transfer*: John Wiley & Sons, 2011.
[32] *Solid Curved Face Ceramic E-Mitters*. Available: http://www.tempco.com/Infrared/Ceramic%20Emitter%20Style%20CRL.html
[33] *TEC Mounting*. Available: http://www.customthermoelectric.com/TECmounting.html
[34] C. C. L. Mahder Tewolde , He Tao, Hanfei Chen, , Gaosheng Fu, Di Liu, Tao Zhang, and L. Z. David Benjamin, David Hwang, Jon Longtin, "Sensors for Small Modular Reactors Powered by Thermaoelectic Generators," in *Proceedings of the ASME 2014 Small Modular Reactors Symposium*, Washington, DC, USA.